ACTIVE CONSTELLATION EXTENSION BASED TRELLIS SHAPING FOR PEAK-TO-AVERAGE-POWER-RATIO (PAPR) REDUCTION IN SISO-OFDM SYSTEMS

by

NS Maryam Azhar

(00000319094)

Supervisor

Asst Prof Abdul Wakeel, PhD

A thesis submitted to the faculty of Electrical Engineering Department Military College of Signals, National University of Sciences and Technology, Rawalpindi as part of the requirements for the degree of MS in Electrical Engineering

APRIL 2022

ABSTRACT

To accomplish the necessity of high data rate, different research groups have proposed different communication technologies. Orthogonal Frequency Division Multiplexing (OFDM) is one of such technologies that has gained admiration and popularity due to its reliable and error-free transmission. OFDM is spectrally effective multicarrier modulation technique for high speed transmission of data through multipath fading channels. However, a major drawback in OFDM is the high dynamic range of the transmit signal, i.e the transmit signal has sporadic high peaks as compared to the mean transmit power. It is expressed as high peak to average power ratio (PAPR), which can significantly degrade the system performance. As most of the electronic devices are peak power limited, thus, passing such a high amplitude signal through the non-linear devices will drive them to work in its non-linear region, resulting in signal clipping. This results in both in-band distortion and out-of-band radiation which degrades the system performance in terms of Bit Error Rate (BER). Different techniques have been proposed to limit these peak excursions. One of such techniques that has been proved to be very efficient in terms of PAPR reduction is Trellis shaping (TS). Trellis shaping has been found capable in terms of PAPR reduction without any increase in the mean power of the transmit signal for moderate computational complexity. Herein, we propose Active Constellation Extension (ACE) based Trellis shaping for PAPR reduction in single input single output (SISO) OFDM systems to further enhance system efficiency in terms of PAPR reduction. Moreover, it has been found in the literature that shaping gain increases with Trellis depth of the shaping code. Therefore, to further improve the system effectiveness, shaping codes of different depths were used as well. The simulation results show that a sizeable PAPR Reduction can be achieved using ACE based TS technique and a gain of almost 2.5 dB can be achieved using 16-state trellis depth of the shaping code. Besides PAPR reduction, a comparative analysis of our proposed system using ACE based TS is carried out with a system without ACE in terms of FER. Simulation results were obtained using hard decision decoding as well as soft decision decoding with BCJR. The simulation results show that our proposed algorithm slightly performs better than the conventional system both for hard decision decoding as well as soft decision decoding.

DECLARATION

I certify that the work "Active Constellation Extension Based Trellis Shaping for Peak-To-Average-Power-Ratio (PAPR) Reduction In SISO-OFDM Systems" exhibited in this thesis has not been submitted in support of any other award or educational qualification either at this institution or elsewhere.

DEDICATION

This thesis is dedicated to

MY BELOVED PARENTS, BROTHERS, SISTERs,

HONORABLE TEACHERS AND FRIENDS

for their love, endless support and encouragement

ACKNOWLEDGEMENTS

All praises be to Almighty ALLAH who showered his blessing and enabled me to complete such an exploration work. First of all, I would especially like to thank my supervisors Dr. Abdul Wakeel for his amazing support, guidance and supervision that he provided throughout the course of my thesis. He helped me a lot in completing my research work and were all the time readily available for guidance throughout my thesis. I would also like to thank my Committee Members for their support and valuable suggestions for my research work. Last but not the least, I would like to express my sincere gratitude to my parents and my siblings to whom I am dedicating this work. This thesis would never have been possible without their kind support, prayers and unconditional love.

CONTENTS

ACRONYMS

ACE	Active Constellation Extension
ADC	Analogue To Digital Conversion
AWGN	Additive White Gaussian Noise
BER	Bit Error Rate
BPSK	Binary Phase Shift Keying
CCDF	Complementary Cumulative Distribution Function
CDF	Complementary Distribution Function
CDMA	Code Division Multiple Access
CP	Cyclic Prefix
DMT	Discrete Multi-tone
FFT	Fast Fourier Transform
IACF	Iterative Amplitude Clipping and Filtering
ICI	Inter Channel Interface
IFFT	Inverse Fast Fourier Transform
ISI	Inter Symbol Interference
LDPC	Low Density Parity Check Codes
LSB	Least Significant Bits
MC-CDMA	Multi Carrier Code Division Multiple Access
ML	Maximum Likelihood
MSB	Most Significant Bits
OFCDM	Orthogonal Frequency Code Division Multiplexing
OFDM	Orthogonal frequency division multiplexing
PAPR	Peak to Average Power Ratio
PTS	Partial Transmit Sequence
QAM	Quadrature Amplitude Modulation
QPSK	Quadrature Phase Shift Keying
SLM	Selected Mapping
TR	Tone Reservation
TS	Trellis Shaping

LIST OF FIGURES

Chapter 1

INTRODUCTION

Data at a speed ranging from 100Mbps to 1Gbps is provided by the 4G systems of mobile communications. To fulfill the rising plea for multimedia communications, future systems of communications should be made such that they support a very high transmission rate of data with high fidelity. In upcoming time, broadcasting communication systems will deliver extremely high data rates in the downlink.

In 4G, numerous schemes of wireless transmission have been proposed for broadcasting in the downlink scenarios. The multicarrier code division multiple access (CDMA), orthogonal frequency division multiplexing (OFDM) and orthogonal frequency code division multiple access provide quick broadcasting of data for communication in wireless systems with good performance of the system in terms of BER. Code division multiple access is used to expand the transmission performance. Direct sequence CDMA and multi-carrier CDMA are the two types of CDMA. The current era comprises of high speed broad-casting of data in cellular communications [1]. Another transmission technique for multi-carrier systems is the orthogonal frequency division multiplexing (OFDM).

1.1 Orthogonal Frequency-Division Multiplexing (OFDM)

The knowledge on OFDM is, nonetheless, very old for certain early examinations. The original paper on OFDM frameworks, was published by Chang in 1966 [2]. His proposed idea was of transferring equivalent streams of information through channels which are directly band-restricted. This transmission consumed proportioned multiplexing but it lacked inter-symbol interference (ISI) and inter-channel interference (ICI). Saltzberg [3], in 1967 extended Chang's principle by using Offset Quadrature Amplitude Modulation (OQAM). In earliest modem, Kineplex [4] and Kathryn [5] were rare examples that used OFDM. Weinstein and Ebert presented a paper [6] in 1971 that was a major innovation in the expansion and growth of the OFDM system. The authors applied DFT/IDFT in OFDM system for modulation and

demodulation of the baseband signal. This DFT, minimized the difficulty through elimination of the oscillator bank of the subcarriers. In 1980, paper by Ruiz and Peled was another significant achievement for the advancement of OFDM frameworks [7].

As the name indicates, OFDM comprises the familiar practice of Frequency Division Multiplexing (FDM). In OFDM, the available bandwidth is divided into orthogonal sub-channels. OFDM is widely used for communication in multi-carrier systems. OFDM achieves high data rates by splitting up the channel into multiple sub channels that transmits data in parallel [8]. Information is carried by closely spaced orthogonal subcarriers. The objective here is to modulate each subcarrier with a different modulation technique (for instance QPSK, QAM) but at a low symbol rate. This low rate is important so that it stays related to the conventional technique of modulation in carriers. OFDM helps in transmission through channels involving frequency selecting [9] . As the name indicates, OFDM is a digital multi-carrier modulation scheme in which orthogonal frequency components are sent for modulation, through multiple subcarriers in parallel, within same single channel. The symbol duration rises sustainably. This problem is sorted out by technique of OFDM with sensible intricacy and high speed of transmission, thus proving it as proficient modulation technique in future systems. For FFT and IFFT, implementation of OFDM is easy. It overpowers the interferences of the narrowband and implements method of multiple antenna so that efficiency can be enhanced. Fig.1.1 shows a simple OFDM generator.

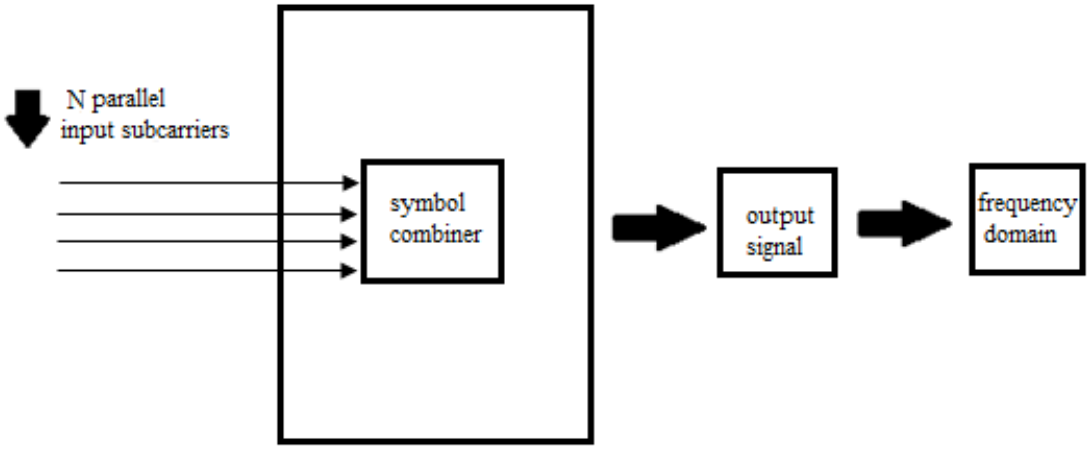

Figure 1.1 Simple OFDM Generator

Input signals of sinusoids, denoted by N, are present in simple OFDM. Each subcarrier transmits one bit information. This shows that every subcarrier transfers N number of bits. Set of orthogonal signal is formed by selection of each subcarrier's frequency.

1.1.1 OFDM Transmitter Receiver

Technique of convolution code encodes the data at input for systems using OFDM. Complex numbers are used to symbolize data which is serial at this time. Pilot mapping technique is used at this moment. Next, the converter is used to convert data from serial to parallel and then parallel complex data is passed through IFFT operation. Transformed data is then assembled for subcarrier transmission. After this procedure, data is multiplexed in serial. Every block of data has cyclic prefixes or the guard intervals for channel's long spread of delay and ISI minimization. However, CP has a drawback of reduction in efficiency of power and channel's spectral containment. After the modulation, digital data is transformed into analog data from digital-to-analogue Converter.

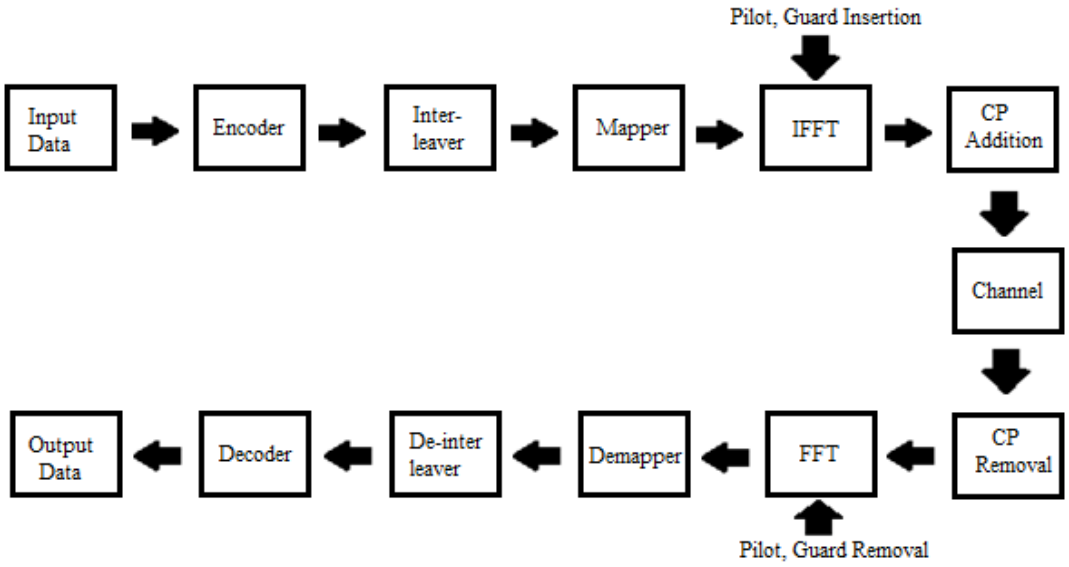

Figure 1.2 OFDM Transmitter Receiver Block Diagram.

At the receiver side, the received signal is converted from analog to digital data from analogue-to- digital Converter. During the down conversion of signal, synchronization is also desired. The OFDM signal is demodulated by using FFT. After the FFT operation, the received data is demodulated. In the end, output data is acquired by decoding. The data is then converted from parallel to serial in last [10]. Transmitter

and receiver for OFDM is given in Fig.1.2.

1.1.2 SISO-OFDM Systems

The expansion in wireless communication poses significant trials to the future broadcasting networks. The numerous antennas are nearly organized in four diverse scenarios that are:

- **Single-Input Single-Output (SISO)** or in other words, a downlink scenario for single user. In SISO systems, the transmitter side has single antenna for transmission of data and receiver side has single antenna for receiving of data.
- **Single-Input Multiple-Output (SIMO)** or in other words, downlink scenario for multi user. In SIMO systems, the transmitter side has single antenna for transmission of data and receiver side has multiple antennas for receiving the data.
- **Multiple Input Single Output (MISO)** or in other words, uplink scenario for multi users. In MISO systems, the transmitter side has multiple antennas for transmission of data and receiver side has single antenna for receiving the data.
- **Multiple Input Multiple Output (MIMO)** or in other words, Point to Point (P2P) scenario for multi users. In MIMO systems, the transmitter side has multiple antennas for transmission of data and receiver side has also multiple antennas for receiving the data.

Here we will discuss SISO systems only. OFDM was initially suggested for SISO systems. In SISO systems single antenna is present at transmitter side for transmission of data and single antenna is present at receiver side for receiving the data as shown in Fig.1.3. This makes SISO the simplest to implement and easiest to design amongst all the types of antennas available. Bandwidth of the SISO system's channel remains restricted by Shannon's law. This law is stated as, maximum rate of transmission of digits that are free in error, over a channel with narrowed bandwidth and noise addition. The benefit of SISO system usage is its very simple and economical design

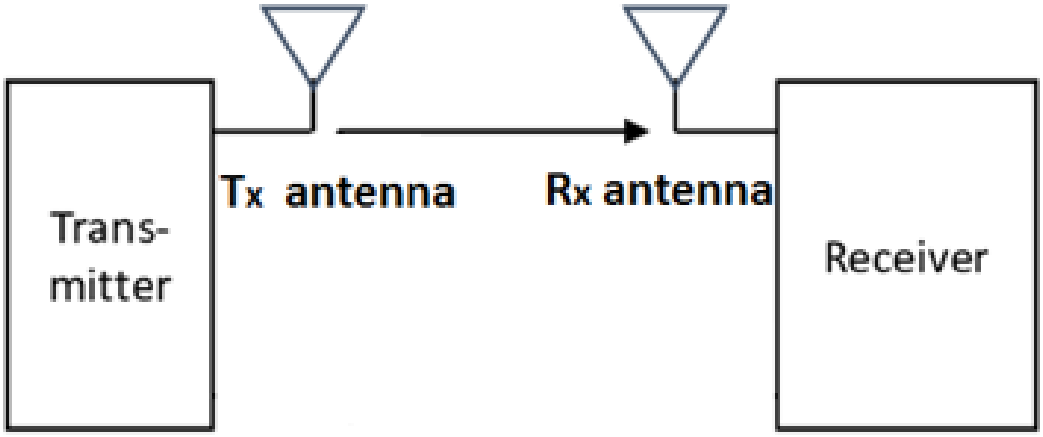

Figure 1.3 Single Input Single Output (SISO) Model

as compared to rest systems. Television, broadcasting of radio and Wi-Fi are the few applications of SISO system. SISO-OFDM technology was embraced world-wide in the beginning as it had high rates of data for frequency channels. For SISO-OFDM systems, multiple symbols are simultaneously transmitted through subcarriers that are orthogonal by single transmitter [11]. Symbols in OFDM systems, consume a comparatively extended duration of time as compared to rest methods of modulation. There is overlapping of subcarriers in the time and frequency domains. The waveforms of signal in OFDM are designed such that they are orthogonal, because each symbol of OFDM is extended cyclically in the time domain. At transmission side, this technique comprises of IFFT and FFT at the receiver side. After FFT operation, the data is received at output via single receiver antenna.

Signal robustness, against selection of frequency, is due to narrowband subcarriers [12]. This happens because of delay spread in multipath. Though, OFDM is comparatively sensitive to time selectivity that occurs as a result of fast variations in time. Inter carrier interference (ICI) arises due to the corruption in orthogonality of OFDM waveforms by time variations. OFDM techniques has numerously been reflected as talented plan to boost capacity, transmission rate of data and worth for broadband wireless structures.

1.1.3 Fundamentals of OFDM

Discrete Fourier transform (DFT) divides the whole bandwidth into N sub-channels for transmission in multi-carriers. In this way, multiple low bit rate streams are

formed from a high data rate stream. The low streams of data are sent through different sub-channels. OFDM signal carrying multiple modulated symbols are formed as a linear combination of complex exponential signals of finite time duration [13]. Mathematical representation of the OFDM signal is:

$$x_n(t) = \sum_{k=0}^{N-1} x_n, k^{e^{j2ptk\Delta ft}}, 0 \leq t \leq T_s \tag{1.1}$$

where T_s shows the symbol duration, Δf for the sub-channel space and N for total number of sub-channels, respectively. Towards the receiving end, in case there is no distortion, the transmitted signal can be detected as:

$$x_{n,k} = \frac{1}{T_s} \int_0^{T_s} x_n(t) e^{-j2pik\Delta ft}\, dt \tag{1.2}$$

Orthogonality condition need to be achieved in order to acquire the detection of data at receiving side. This condition states that the length of symbol duration should be such that, the subcarriers are orthogonal to each other for different values of K. An additional feature of OFDM is that the same QAM constellation isn't necessary for all $[X_n]$ therefore, different modulation schemes can be used simultaneously. Bit loading and power loading are some of the modulation schemes used for various modulation schemes [14]. Then the OFDM signal is achieved by serial to parallel conversion. This converts the serial data into a parallel stream. N-point IDFT (IFFT) modulator converts this data stream into time domain, such that:

$$[x_k] = IDFT[X_n] = \frac{1}{\sqrt{N}} \sum_{n=1}^{N} X_n e^{j\frac{2\pi nk}{N}}, k = 1, 2, ..., N \tag{1.3}$$

where x_k is for the k_{th} sample while N shows the OFDM block length. Symbols are converted to time domain by the modulator of IDFT modulator. The symbols are then re-converted to data in serial by a P/S converter. Cyclic prefix is appended before transmission. At the receiver, firstly the removal of cyclic prefix takes place. The signal y_k is converted from serial to parallel data stream. DFT of the symbol is

obtained. Lastly, the received symbols are demodulated as:

$$[Y_n] = DFT[yk] = \frac{1}{\sqrt{N}} \sum_{k=1}^{N} [yk] e^{-j\frac{2\pi nk}{N}}, n = 1, 2, ..., N, \tag{1.4}$$

The transmitted symbol x_n, k is received as:

$$x_{n,k} = \frac{1}{T_s} \int_0^{T_s} x_n(t) e^{-j2pik\Delta ft}\, dt \tag{1.5}$$

1.1.4 Advantages of OFDM

OFDM has the potential for high rate of data transmission and moderate equalization of complexity. So, OFDM has been selected for countless recent wireless and wireline standards of communication for SISO systems. OFDM restricts the interferences of the narrowband channels and executes practices of multiple antenna to improve efficiency. It is also a running candidate for the proposed 5-G communication technology [15]. OFDM is one of the principal contenders for coming wireless systems. OFDM possess benefit over single-carrier systems because of its capacity to deal with with severe channel situations without complex filters of equalization. OFDM has plentiful advantages and applications in wireless communication networks, 4G/5G mobile communication, digital video and audio broadcasting (DVB/ DAB). Besides, OFDM have a number of commercial applications for instance Digital Subscriber Line (DSL), DVB-H, and MediaFLO, e.t.c. It bears high spectral efficiency, adaptable resource allocation and robustness against Inter-Symbol Interference (ISI). OFDM is of major importance because of its ability to deal with the issues of multi-path propagation, high data-rates, and bandwidth efficiency.

1.2 PAPR in OFDM

A main problem of OFDM is the non-constant envelope of the signal that is transmitted. If this issue is not treated, the OFDM signal gets a large peak-to-average power ratio (PAPR), causing challenges for amplification of power in the transmitter. High PAPR

degrades performance of OFDM signals by forcing the nonlinear devices to operate in its nonlinear region, resulting in distortion and clipping of the signal which degrades system performance [16].

High PAPR of OFDM system is delicate to non-linearity of high power amplifiers. The peak power of M-QAM modulated symbols is expressed as:

$$P_{QAM} = \frac{\alpha^2}{2}(\sqrt{M} - 1)^2 \tag{1.6}$$

The peak to average power ratio (PAPR) is the ratio of the signal's peak power to the signal's average power. This shows the extent of amplitude fluctuations for a signal. PAPR is given by:

$$PAPR(x) = \frac{Peakpower}{Averagepower} = \frac{\max_{k,1\leq k\leq N}|x_k|^2}{E\{|x_k|^2\}} \tag{1.7}$$

Here, $max|x_k|^2$ is representing the highest amplitude of peak of power for the envelope. The average power is denoted by E$\{|x_k|^2\}$ from $1 \leq k \leq N$ interval of symbol x for OFDM.

1.2.1 CDF and CCDF Analysis

Let the k_{th} sample's PAR be τ_k, then there is a probability of PAR to be less as compared to the value of threshold that is τ [17]. This is shown as:

$$CDF(PAR) = Pr(\tau k \leq \tau) \tag{1.8}$$

The CDF with N samples for an OFDM frame can be given by:

$$CDF_\tau(\tau) = (CDF_{\tau k}(\tau))^N = (1 - e^{-\tau})^N \tag{1.9}$$

Overhead equation can be used to express the equation of Complementary Cumulative Distribution Function. CCDF is the possibility of PAR in OFDM to be larger than the threshold τ. For single antenna in OFDM system, equation for CCDF at Nyquist rate

is:

$$CCDF(PAR) = P_r(PAR > \tau) = 1 - (1 - e^{-\tau})^N \tag{1.10}$$

1.2.2 Consequences of High PAPR

High PAPR of OFDM causes high dynamic range of transmitted signal in time domain. The time domain transmit signal has sporadic peaks much higher than the average power of the signal. As most of the electronic devices are peak power limited, thus passing such a high amplitude signal through the non-linear will drive them for functioning in the non-linear region, resulting in the signal clipping. To solve this issue, expensive linear amplifiers of power can be used or nonlinear amplifiers with high back-offs can be used, to exclude substantial out-of-band radiation, inter-modulation of subcarriers in OFDM and degradation in BER performance. This points to inefficient amplification of power, being critical for devices that are supplied with battery power. The counter measure is either to operate the non-linear devices with high power back-offs. Actions are essential for restricting these peak excursion before transmitting them through the non-linear devices. To limit the occurrence of high peaks, different algorithms have been proposed by different authors, discussed later.

1.3 Problem Statement

High PAPR degrades performance of OFDM and reduces efficiency of the system. If the peaks are not minimized, the non-linear device may clip it causing signal distortion resulting in system performance degradation in terms of bit error performance. Among many proposed techniques, we are using Trellis Shaping technique for PAPR Reduction as this technique gives the better result as compared to rest techniques. To further improve the gain and BER of the system we will be combining Trellis Shaping with Active Constellation Extension, which will be discussed later. Also, the peaks of signal in time domain are cancelled by modifications in constellation. This helps in little performance degradation with a slight increase in computational complexity.

1.4 Goals and Objectives

The research objectives of the suggested work are following:

1. To go through different PAPR reduction techniques that are available
2. To develop a hybrid PAPR reduction algorithm that is Active Constellation Extension based Trellis Shaping
3. To evaluate the performance of the proposed scheme with different trellis depth of the shaping code
4. To get optimization of the distribution of degree for variable node in irregular LDPC codes, that are concatenated with the Trellis Shaping

1.5 Significance of the Research

High PAPR in SISO-OFDM systems cause less efficient system with high power consumption along with degradation in performance. This changes the regions of decision in maximum-likelihood (ML) and increases the BER. So we needed a system to show that the PAPR reduction in SISO-OFDM systems, desires an additional efficient solution than application of the existing schemes for OFDM systems. Thus hybrid scheme of TS with ACE helps in reduction of peaks of signal avoiding complexity and BER. The method in this research, adjusts the signal constellations in domain of frequency such that the PAPR of signal in the domain of time, is minimized.

1.6 Advantages of Research

In this research, we are using Active Constellation Extension based Trellis Shaping for peak Reduction and gain improvement. Following are its advantages:

1. A hybrid scheme can be achieved, which will improve the performance of TS in terms of PAPR.
2. The performance can further be improved using trellises of different depths.
3. Using optimized LDPC code will enhance system performance in terms of BER

4. TS involves decoding metric and sequential decoding, which will help to recover PAR and complexity reduction.

5. TS minimizes the side-lobe components of autocorrelation and thus can reduce the PAPR and as well as average power of the signal system.

6. ACE does not changes the decision regions of maximum likelihood (ML) and neither increases the bit-error rate (BER).

7. The future wireless networks will be highly operable with provision of connectivity to multiple technologies and protocols part of the same network.

1.7 Application Areas

This hybrid technique is very useful for:

1. Wifi

2. 5-G wireless communication

3. DMT communication

4. any wireless communication using multicarrier systems

Chapter 2

LITERATURE REVIEW

Signal transmitted in OFDM have a drawback of high PAPR. If these peaks are not minimized then this may result in degrades performance degradation of OFDM and reduction of system efficiency. In the present literature, rising number of practices have been suggested to resolve the difficulty of power efficiency like:

- Clipping and Filtering [18–21]
- Selected Mapping (SLM) [22–26]
- Partial Transmit Sequence (PTS) [27–30]
- Tone Reservation (TR) [31–34]
- Trellis Shaping (TS) [35–39]
- Active Constellation (AC) [40–42]

In this chapter, we present literature review, basic overview of PAPR Reduction techniques and their implications for communication systems. Herein, we will provide a brief discussion to some of the well-known approaches used for PAPR reduction in SISO-OFDM systems.

2.1 Clipping and Filtering

At first, Iterative Clipping and Filtering (ICF) conventional techniques were proposed by X. Li, A. Gatherer and J. Armstrong [18, 19] for PAPR Reduction in single input single output (SISO) systems. In this technique, peaks of signal crossing a certain threshold value were clipped to limit the peak excursions. To avoid spectral spreading, the clipped signal was passed through an IFFT/FFT pair working as filter. Several iterations were required to lessen the peak regrowth for this technique. So, multiple iterations had to be performed in the ICF scheme which led to a large number of fast

Fourier transform (FFT) operations, causing high implementation complexity. Block diagram of ICF is given in Fig.2.1.

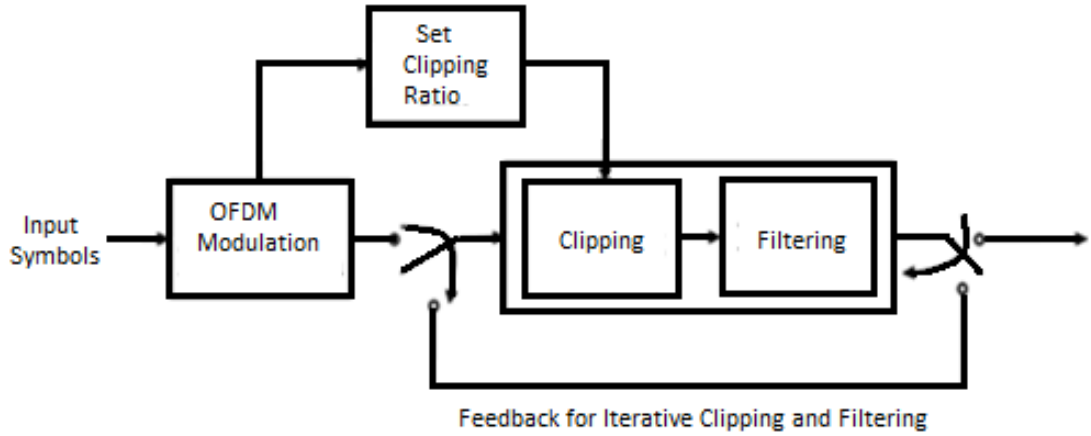

Figure 2.1 Clipping and Filtering Block diagram

To solve this issue, a modified Iterative Amplitude clipping and filtering (IACF) technique [20] was introduced to reduce the PAPR in communication signal system. This technique helped in the PAPR reduction using band-limited filter in the ICF. This improved method and achieved the target PAPR using fewer iteration numbers and enhanced the PAPR and BER performance as compared to the conventional method [21]. However, ICF is computationally complex, as it involves many DFT operations and the algorithm also cause signal distortion, resulting in BER degradation.

2.2 Selected Mapping (SLM)

Due to its simplicity for implementation, SLM technique is a favorable technique which presents no distortion in the transmitted signal. In SLM technique, PAPR that is lowest, is nominated among set of adequately different signals which are all indicating the similar data. SLM is a flexible technique as it is a limit-free technique on subcarrier modulation. Block diagram of SLM is given in Fig.2.2.

In [22, 23], Fischer, Muller and Huber proposed Selected Mapping (SLM) for PAPR Reduction in SISO-OFDM systems. In this technique, a set of candidate sequences bearing the same information, were generated and then the one with the least PAPR was selected for transmission [24]. However, a major concern of the SLM is that the

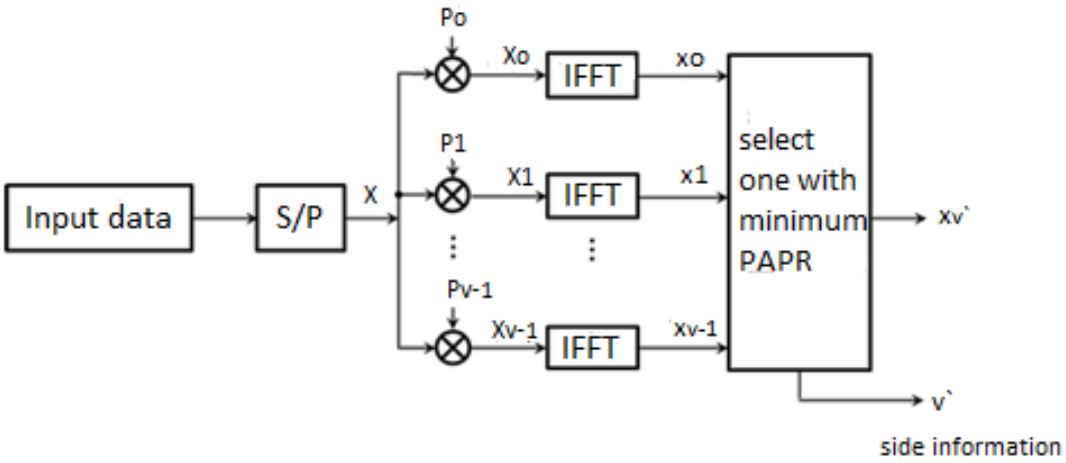

Figure 2.2 Selected Mapping (SLM) Block diagram

increase in number of candidate frames cause the proportional escalation in the IFFT. This makes the system computationally complex [25, 26].

2.3 Partial Transmit Sequence (PTS)

Likewise SLM, Partial Transmit Sequence (PTS) was introduced by Fischer and Muller in [27]. In PTS, each input data block was divided into non-overlapping sub blocks and were independently multiplied with the rotation factor that generated time domain data with lowest amplitude. PTS was modified by Huber and other authors [28] to temporally shifted PTS, directed PTS and hybrid PTS. In these methods, the sub blocks were multiplication of sub-blocks was performed by different factors of phase weighing. Then these sub-blocks were summed together for production of candidate signal with lowest PAPR. These methods had better simulation results then SLM, however, PTS technique had the drawback of exhaustive search which increased the computational complexity as the number of sub-blocks increased [29].

PTS is unique techniques which gives worthy PAPR reduction for OFDM signal systems. In PTS wide random search is done among every combination of the allowable phase vectors due to which it has high complexity. Increase in phase vectors numbers, result in the exponentially raise of search complexity. PTS is observed as a distortion-less technique because it depends on the method of scrambling signal for reduction of the value of PAPR [30]. So, the PTS technique fixes the problem of the

distortion of power signal and degradation in bit error rate (BER).

Among rest techniques, PTS is numerous signal illustration techniques that splits the block of data into some groups. These groups are jumbled to pick the signal of transmission. PTS technique, partitions the data symbols at input into the separate subsets which are having different factors of rotation and are rotated differently. This helps in improvement of partitioned subsets and these improved subsets are once again to make candidate signals set, namely PTS. At last, the sequence with least value of PAPR is selected for the transmission of data. Block diagram of PTS is given in Fig.2.3.

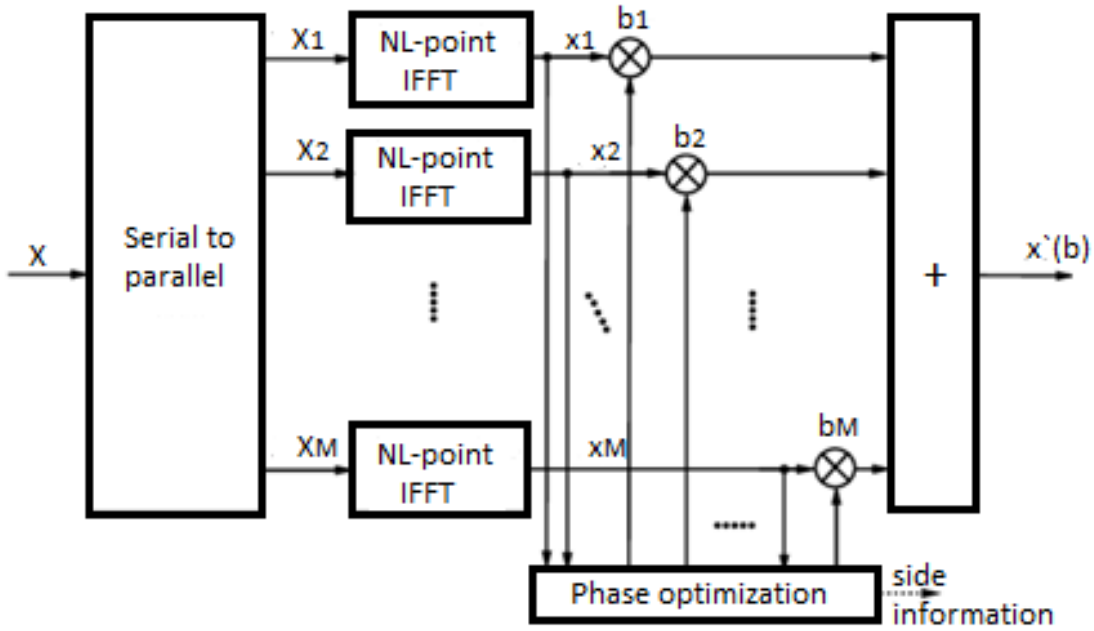

Figure 2.3 Partial Transmit Sequence (PTS) Block diagram

2.4 Tone Reservation (TR)

Tellado, in [31], proposed Tone Reservation technique for SISO-OFDM systems. In TR algorithm, a corrective signal is generated on a set of reserved tones. This corrective signal is then iteratively added (subtracted) in the domain of time to the transmitted signal for reducing the PAPR [32, 33]. However, a major drawback with TR is that the mean power of the transmit signal increases with addition or subtraction of the corrective signal for PAPR reduction. Besides rise in the mean power, there is loss in the capacity of channel because the reserved tones transmit no data.

In TR algorithm, signal is dependent on input data and this data signal is increased in time domain to the original signal for peak decrease. By utilizing a certain tones that are reserved for PAPR, time domain signal is generated. The algorithm is used to divide the tones in two disjoint sets from OFDM frame. . Block diagram of TR is given in Fig.2.4.

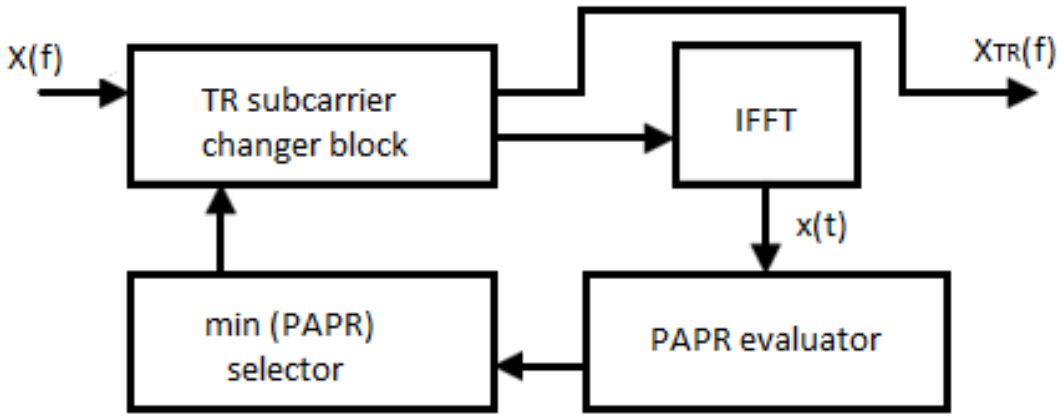

Figure 2.4 Tone Reservation (TR) Block diagram

2.5 Trellis Shaping (TS)

Werner Henkel, in [34], proposed Trellis Shaping for PAPR reduction in multicarrier systems. The idea of Trellis Shaping was firstly offered by G. D. Forney [35] for mean power reduction. In [36], the authors proposed two matric in the Viterbi algorithm for search. First was in time domain and the second was in frequency domain. The time domain matrix had good results at the cost of additional complexity. To deal with the system complexity, H. Ochiai [37] proposed a matric in frequency domain based on minimization of the auto-correlation of the side lobes. The authors have showed in [38, 39] that a considerable gain can be obtained with their proposed matric. Block diagram of TS is given in Fig.2.5.

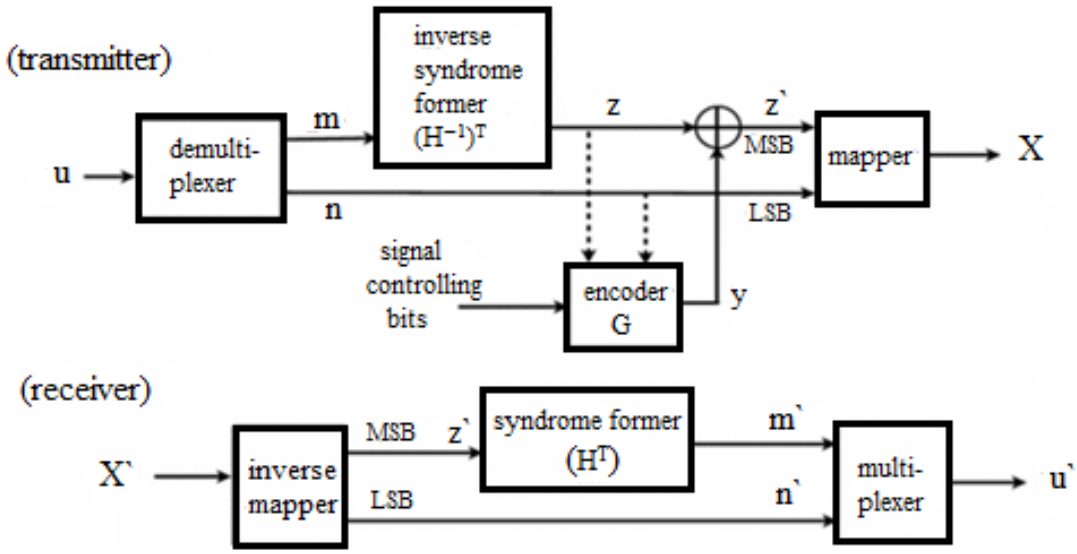

Figure 2.5 Trellis Shaping (TS) Block diagram

2.6 Active Constellation (AC)

This technique was proposed by D. L. Jones [40] for PAPR Reduction. He proposed PAPR Reduction in OFDM and discrete multi-tones (DMT) via active channel modification. In ACE, the outer constellation points are extended outwards and then convex optimization is used to find the set of extended constellation points that minimize the PAPR. Fig.2.6 shows the extension of outer constellation point for 4-QAM and 16-QAM. With the help of this method, bit error rate was decreased slightly while significantly reducing the magnitudes of peak. The proposed technique is computationally complex. Later, S. Krongold and G. R. Woo B [41, 42] worked on OFDM's PAR reduction by ACE for further improved results. This method is very efficient but is very time consuming. Moreover, extending the outer constellation points results in an increase in the average power.

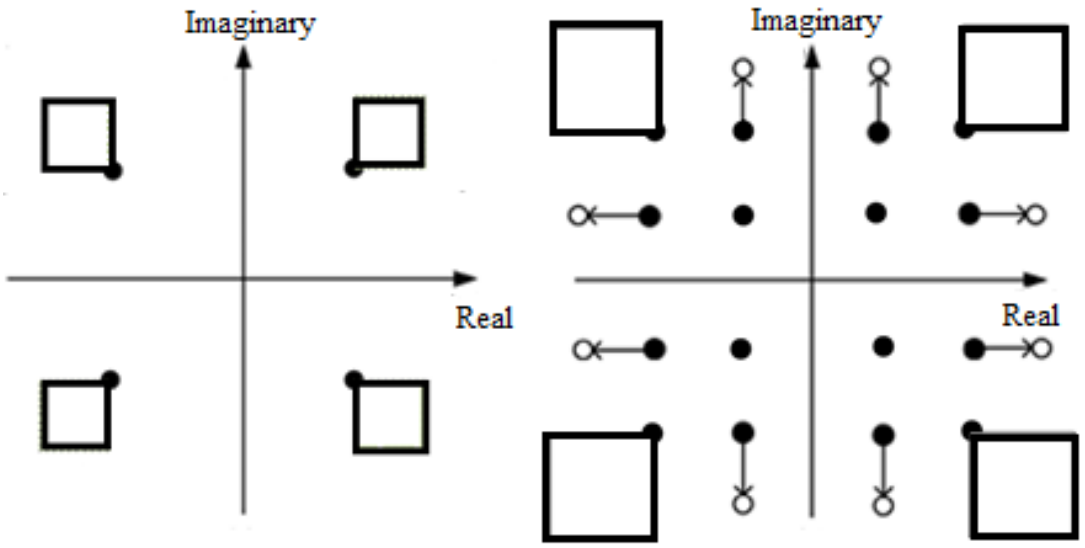

Figure 2.6 Constellation mapping for the sign-bit shaping (4 QAM and 16-QAM)

Chapter 3

ACTIVE CONSTELLATION EXTENSION BASED TRELLIS SHAPING

We have briefly explained the proposed techniques used for PAPR Reduction before, among which Trellis Shaping has better results as compared to the rest. In this chapter we will discuss in detail about Trellis Shaping and Active Constellation Extension. We will also discuss the proposed hybrid Active Constellation Extension based TS technique for this research. To improve our results in terms of system performance, we will use shaping codes of different trellis depth. Other than the peak reduction, we will also optimize the variable node degree distribution by exploiting the individual bit error probability of higher order QAM constellation for LDPC codes.

3.1 Trellis Shaping (TS)

The original scheme of TS was firstly given by the author named G. D. Forney [35]. Minimization of the average power of the transmitted sequence was done by him. The average power was reduced by addition of a sequence of code of modulo 2 of the shaping code Cs with the sequence of data represented by u. Viterbi algorithm is used for this addition and it is based on branch metric. Mean power was utilized as branch metric by Forney, for the Viterbi algorithm. In this research, we will reflect shaping of side bits along with binary code of convolution [43]. TS is a technique used for reduction in the PAPR of the band-limited OFDM signals. This methodology is built on recursive minimization of the auto-correlation of side-lobes in data sequence of OFDM. An innovative metric in combination with the Viterbi algorithm is deliberated.

3.1.1 TS Transmitter Receiver

System model for TS has the transmitter side and receiver side. Before constellation mapping, the input sequence of data is represented by u, which is transmitted with N-subcarrier symbol in OFDM. At the transmitter side, first the input data (u) is send to demux where it divides into two sequences. One gives the MSBs and the other

gives the LSBs. This sequence represented by u is involves two sequences that are m and n. m represents the MSBs, that are the sign bits of the mapping constellation and n represents the LSBs that are the least significant bits. For choosing the MSBs, the sequence of input data is pre-processed by the syndrome former's left inverse. The MSBs and LSBs, after passing through Viterbi decoder, are sent for QAM mapping. After that IFFT operation is performed [44].

At the receiver side, the FFT operation is performed and the received data is sent for QAM de-mapping. This results in two sequences again: MSBs and LSBs. In LSBs case, no processing was done at the side of transmitter, so LSBs are straightly mapped to the bits of input in correspondence. However, the MSB sequence (m‘) is sent to syndrome former matrix to get the required result and then it is sent to Mux. After the Mux, we get the output sequence (u‘) at receiver side. Fig.3.1 shows the block diagram for trellis shaping:

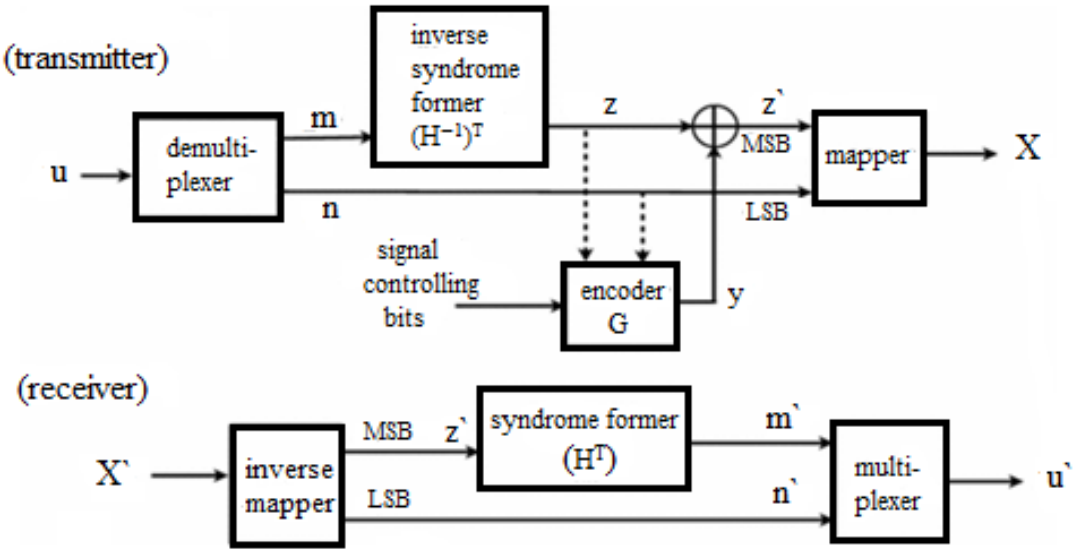

Figure 3.1 Trellis Shaping Block Diagram

3.1.2 System Model for TS

In Fig. 3.1, Cs represents the rate-k/n code of convolutional or the shaping that has a generator matrix G of $k*n$ order. The parity-check matrix also known as syndrome former of order $n*(n-k)$ and its left inverse of order $(n-k)*n$, is represented by H^T and $(H^{-1})^T$. For the shaping of the sign bits, convolutional code Cs of rate-1/2 is used along with generator matrix G of order 1×2. The dimensions of matrix for syndrome former is

2×1 and for its inverse syndrome former is 1×2. Before constellation mapping, the input sequence of data is represented by u, which is conveyed with symbols of N-subcarrier in OFDM [45]. Two sequences are included in sequence u that are m and n. As shown in figure, m gives the MSBs or the signed bits of the constellation of mapping, and n represents the least significant bits denoted as LSBs. For the MSBs, the sequence m is first preprocessed by the syndrome former's left inverse $(H^{-1})^T$ and the sequence z is obtained. Z sequence is then added to a sequence of valid code represented by y. Cs is the binary code of convolutional for shaping

$$z = m(H^{-1})^T \tag{3.1}$$

$$z' = z \oplus y \tag{3.2}$$

After mapping of input data for OFDM, the symbols of QAM are changed to time domain by modulator via IFFT operation. The x signal is transferred from a channel of noise to receiver side. For the receiver end, the estimated $\hat{x}$ is transformed to discrete fourier transform domain by means of demodulator using FFT operation. After the decoding of the symbols $\hat{X}$ by hard decision, the key goal of the receiver is to decode the bit sequence of receive data to get MSBs and the LSBs. In LSBs case, no processing was done at the side of transmitter, so LSBs are right away mapped to the bits of input in correspondence. For receiving the MSBs z', we initially recollect some elementary definitions from theory of coding of the channels. A valid code sequence $y \in Cs$, is obtained for a convolutional code Cs with a generator matrix:

$$y = iG \tag{3.3}$$

where, i is representing the arbitrary sequence of input bits and G is representing the generator matrix of Forney such that the condition $GH^T = 0$ is fulfilled. Furthermore, y will be a valid code sequence in Cs when:

$$yH^T = 0 \tag{3.4}$$

where, syndrome former is showed by H^T for Cs. For getting back the m input sequence, the z' is treated with H^T, i.e.:

$$z'H^T = (z \oplus y)H^T = zH^T \oplus yH^T \tag{3.5}$$

$$z'H^T = zH^T \oplus 0 = m(H^{-1})^T H^T \tag{3.6}$$

$$z'H^T = mI = m, \tag{3.7}$$

where $(n-k)*(n-k)$ identity matrix is represented by I.

3.1.3 Metric Design of TS for OFDM Signal

As we know that TS involves minimization of the auto-correlation of the side lobes. We will minimize the absolute value of the side-lobes instead of reducing their absolute value [70].

$$y = \arg min_{y \in C_s} \sum_{m=1}^{N-1} |R_m|^2 \tag{3.8}$$

The quantity of subcarriers are organized by each shaping symbol. The shaping symbol is represented by y_k. It is chosen at *lth* stage according to

$$y_k = \arg min_{y_k \in C_s^k} \mu^{(i)} \tag{3.9}$$

Where C_s^k denotes set of the *kth* output symbols of the shaping code and u(i) is defined as:

$$\mu^{(i)} \triangleq \sum_{m=1}^{i-1} |R_m^{(i)}|^2 \tag{3.10}$$

For the sign-bit shaping case, and the following recursive relationship can be easily derived:

$$R_m(i) = R_m^{(i-1)} + \delta_m^{i-1} \tag{3.11}$$

where

$$\delta_m^{(i)} \triangleq A_i A_{i-m}^* \tag{3.12}$$

Substituting Rm value in $\mu(i)$ equation, $\mu(i)$ can be expressed in the following recursive form:

$$\mu^(i) = \mu^{(i-1)} \sum_{m=1}^{(i-2)} 2\Re\{R_m^{(i-1)} * \delta_m^{(i-1)}\} + \sum_{m=1}^{(i-1)} |\delta_m^{(i-1)}|^2 \tag{3.13}$$

For above equation, the third term on right side, shows the function of the power of symbols in the subcarrier. This function stays constant for the Type-I mapping [71] and thus, can be omitted for mapping strategies. Viterbi algorithm selects the minimal path of every state, after which the autocorrelation can be revised. Next metric is calculated using this value. Each state should store and refer to all the previous symbols of subcarrier in accordance with the pathway that is the chosen. So, the required calculation complexity of the metric, is significantly higher than the typical Viterbi decoder.

3.1.4 Performance of TS

The performance of the TS is be determined by strategy based on mapping of signals. The two types of mapping strategy are:

1. **Type-I**
2. **Type-II**

The Type-I mapping strategy lacks the capability of the average power reduction, but it can attain a substantial reduction of the PAPR. Whereas, the Type-II mapping strategy is deliberated such that it can accomplish the reduction in peak and average power. Type-I and Type-II mapping of the signals gives the LSBs as shown in Fig.3.2. System's probability of BER through a channel of AWGN is assessed, basing on simulations which approves the efficiency of the projected scheme.

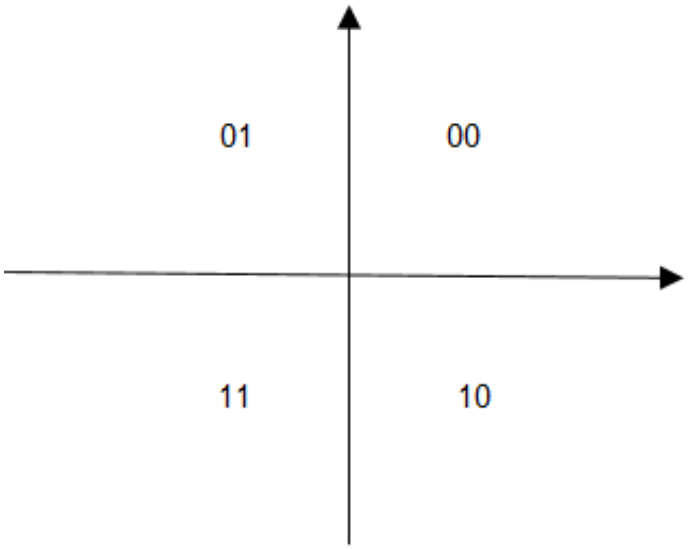

(a)

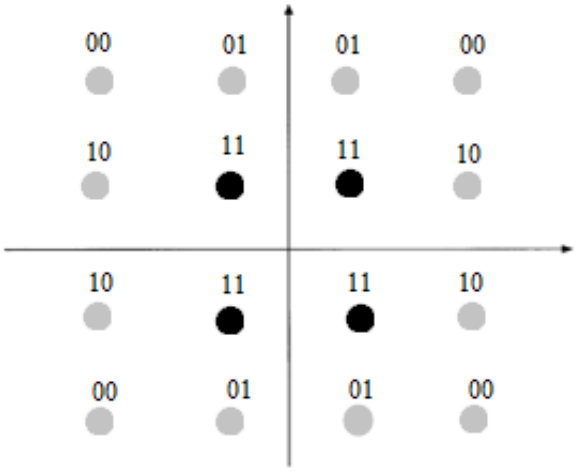

(b)

(c)

Figure 3.2 Constellation mapping for the shaping of the sign-bits in 16-QAM: (a) MSB, (b) LSB: Type-I, and (c) LSB: Type-II.

3.2 Active Constellation Extension (ACE)

In ACE, the outer constellation points are extended outwards and then convex optimization is used to find the set of extended constellation points that minimize the PAPR. This scheme simultaneously decreased the bit error rate slightly while substantially reducing the peak magnitude [46]. For ACE scheme, the peak of signal is decreased through appropriate extension of the outer boundaries of constellations in signal for frequency domain. The modifications in constellation helps to cancel the peaks of time domain for transmitted signal. This is completed with no performance degradation and with little rise in the average power of the transmitted signal.

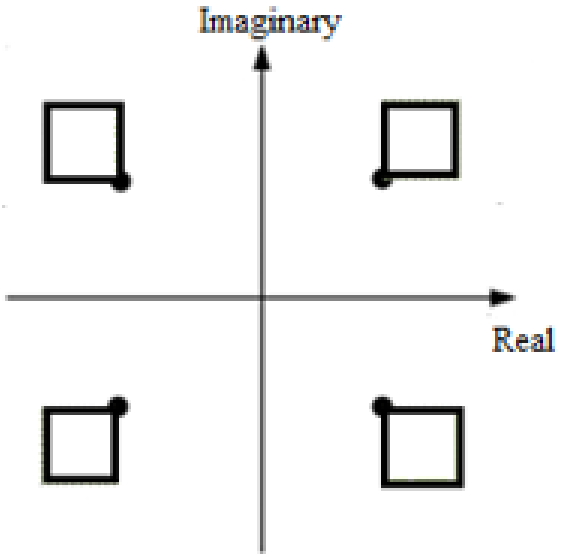

Figure 3.3 Depiction of ACE with QPSK encoding

The shaded regions in Fig.3.3 and Fig.3.4, represent corner-point extension regions and the dotted arrowed lines represent the extension paths for side points. Effectiveness of ACE method can evidently be seen for small constellations like for Quadrature Phase Shift Keying QPSK, all the subcarriers can be extended, but for 16-QAM, only small part of the subcarriers can be extended. The ACE scheme is also suitable for other constellations like constellations of M-PSK. For M-PSK, outer constellations boundaries have data points that give them area for enlarged margin. This avoids the degradation of probability in error for rest data symbols [47]. For Binary Phase Shift Keying BPSK, modification of the constellation point within the equal or greater space from the decision boundary is satisfactory. However, the square QAM include either interior, corner, or side points constellation. Interior points are unable to move, side

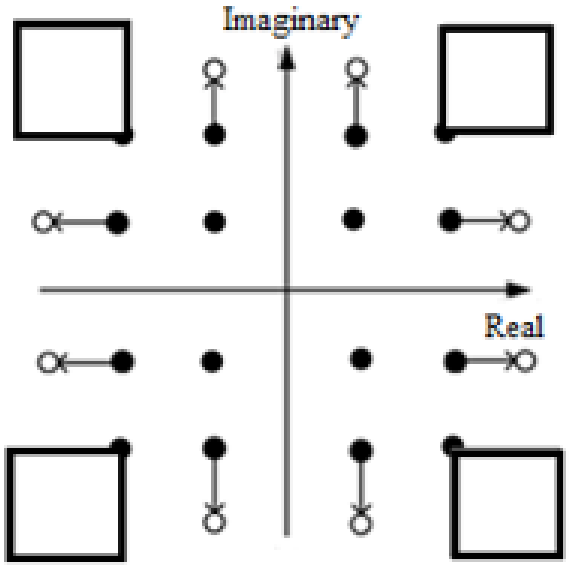

Figure 3.4 Depiction of ACE with 16-QAM encoding

points are only moved outward in one of the direction, whereas the constellation points in corner have a tendency to be moved in outer two directions.

3.2.1 Metric Design of ACE for OFDM Signal

Discrete baseband form for OFDM in time-domain can be expressed as:

$$x_n = \frac{1}{\sqrt{N}} \sum_{k=0}^{N-1} X_k e^{j2\pi \frac{kn}{JN}}, n = 0, ..., JN-1, \tag{3.14}$$

The scheme of ACE adds distortions on subcarriers that are already modulated for reduction in peak of power for OFDM symbols. After the distortion, signal is given by:

$$\hat{x_n} = x_n + d_n = \frac{1}{\sqrt{N}} \sum_{k=0}^{N-1} (X_k + D_k) e^{j2\pi \frac{kn}{JN}} \tag{3.15}$$

where nth sample distortion and the *kth* subcarrier distortion is represented by d_n and D_k respectively. To measure the degree of power variation, the PAPR isgiven as follows:

$$\varepsilon = \frac{max_{[n \in 0, JN-1]} |\hat{x_n}|^2}{E\{|X_k|^2\}} \tag{3.16}$$

In above equation, the denominator is the primitive by which variations in quantity of reference are eluded. This is initiated due to the rise of the signal's power after the ACE.

The minimization of signal peaks can be simplified as a reduction of the maximum power because the average power in OFDM remains constant during the iteration. The peak reduction is formulated as:

$$minimize_D \|x + fD\|_\infty^2 \tag{3.17}$$

where $x = [x_0, \ldots, x_{JN-1}]^T, D = [D_0, \ldots, D_{N-1}]^T$, and f means IFFT operator.

3.3 ACE based TS

A major drawback of multicarrier systems (OFDM/DMT) is high PAPR which is limiting its way to be adopted in different wireless communication technologies. Therefore, measures should be taken to reduce PAPR [48]. Different algorithms have been proposed by different authors for PAPR Reduction with every technique having their pros and cons, like some of them are computationally complex (SLM, PTS or any technique using convex optimization), some require reserved capacity (tone reservation) and some result in performance degradation (clipping and filtering). However, TS has been found out to be computationally less complex and it does not increase mean power nor in system performance degradation (BER).

In this research we propose a hybrid PAPR reduction algorithm: Active Constellation Extension based Trellis Shaping for PAPR Reduction. TS is based on minimization of the auto-correlation of the side lobes. Moreover, in ACE, PAPR is reduced by extending the outer constellation points and convex optimization techniques are used to find an optimum solution [49, 50]. Therefore, taking the idea of constellation extension and using TS to minimize the auto-correlation of the side lobes of the extended constellation point will help in an improved performance of TS with a slight escalation in the complexity of computation. Also, the modifications in constellation cancel the peaks of transmitted signal in time domain with little performance degradation.

3.4 Shaping Codes with Different Trellis Depth

In this research, we will be using shaping codes of different trellis depth which will further improve the system performance in terms of PAPR Reduction. For example, we can plot our ACE based TS results for 4-state, 8-state and 16-state of different subcarriers like 32, 64 and 128 subcarrier and M-QAM. We can also perform PAPR Reduction of different states for different window sizes of 32, 64 and 128. We will compare the PAPR results for same complexity and window sizes of these states and will try to get minimum gain as possible. We will also generate BER curves for these shaping codes and will try to achieve maximum increase in BER performance and system efficiency. Shaping codes are used to shape the M-QAM constellation for PAPR reduction. Herein, a 16-QAM and 256-QAM constellation with Gray mapping is considered with a shaping code of varying trellis depths. By increasing the depth of the trellis (constraint length), we may get some significant improvement in PAPR reduction. These shaping codes are characterized by their Generator matrix G, syndrome former H^T, and its left inverse syndrome former $(H^{-1})^T$. Now let's go through the multiple shaping codes that we have used here for our results.

3.4.1 The 4 State Trellis (5, 7) Code

The trellis with 4 states, in octal refers to (5, 7) in decimal notation. The encoder of this system has 2 memory units or shift registers as shown in Fig.3.5.

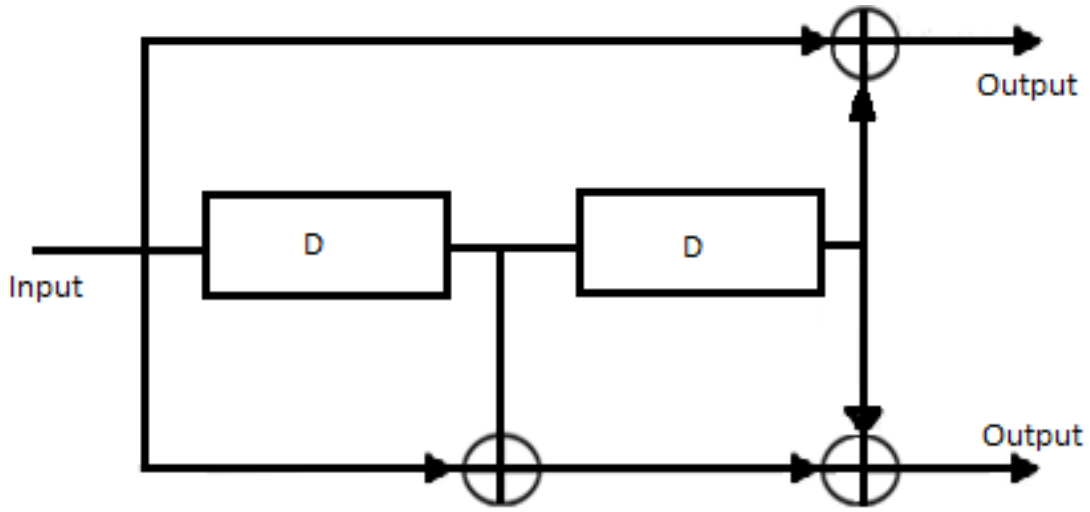

Figure 3.5 Convolutional Code for (5, 7)

The Generator matrix of 4-state code is given as:

$$G = [1 + D + D^2, 1 + D^2] \tag{3.18}$$

At transmitter side, parity check matrix of this shaping code is denoted by (H^T) and its inverse syndrome former matrix is denoted by $(H^{-1})^T$ at the receiver side. This inverse syndrome former is employed to encode the bit stream which forms the MSBs whereas LSBs are passed directly without encoding.

3.4.2 Bit Error Probability 4 State Trellis

For the bit-error probability of 4 state trellis, union bound is applied for approximation. The error probabilities of the bits previously encoded by $(H^{-1})^T$ are now found by exploiting the Union bound. The equation for union bound is based on a few parameters that are: d_{free}, which is the code's minimum hamming distance, A_d which is code's weight distribution and lastly pd which is the likelihood of a wrongly chosen path at distance d. Summation of the error probabilities of the input bit sequence over all paths across distance d is given by union bound. The equation is as follows:

$$P(E) = \sum_{d}^{\infty} A_d P_d \tag{3.19}$$

The probability of choosing a wrong path at a distance d considering an AWGN channel is:

$$P_d = \frac{1}{2} erfc(\sqrt{\frac{E_s}{N_0} d}) \tag{3.20}$$

Here, E_s/N_0 shows the signal-to-Noise ratio in AWGN channel. The general equation for the bit-error probability is:

$$P(b) \approx \frac{1}{k} \frac{1}{2} B_{d_{free}} (e^{\frac{-E_s}{N_0}})^{d_{free}} \tag{3.21}$$

3.4.3 The 8 State Trellis (13, 15) Code

The (15, 17) shaping code in octal refers to (13, 15) in decimal notation and forms a trellis with 8 states. The minimum hamming distance d_f for this shaping code is 6. The encoder of this system has 3 memory units or shift registers as shown in Fig.3.6: The Generator matrix of 8-states code is given as:

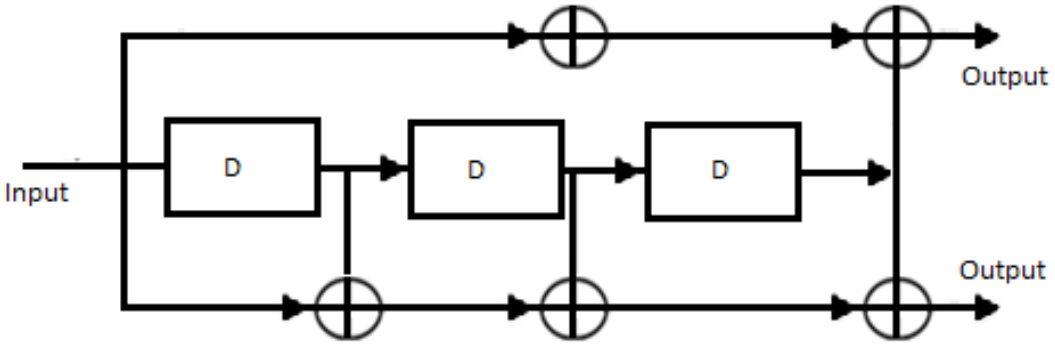

Figure 3.6 Convolutional Code for (13, 15)

$$G = [1 + D^2 + D^3, 1 + D + D^2 + D^3] \tag{3.22}$$

This shaping code's parity check matrix H for (13, 15) is given in Fig.3.7. Its equation is given as:

$$[H^T] = [1 + D + D^2 + D^3, 1 + D^2 + D^3] \tag{3.23}$$

The shaping code's inverse syndrome former for (13, 15) is given in Fig.3.8. Its

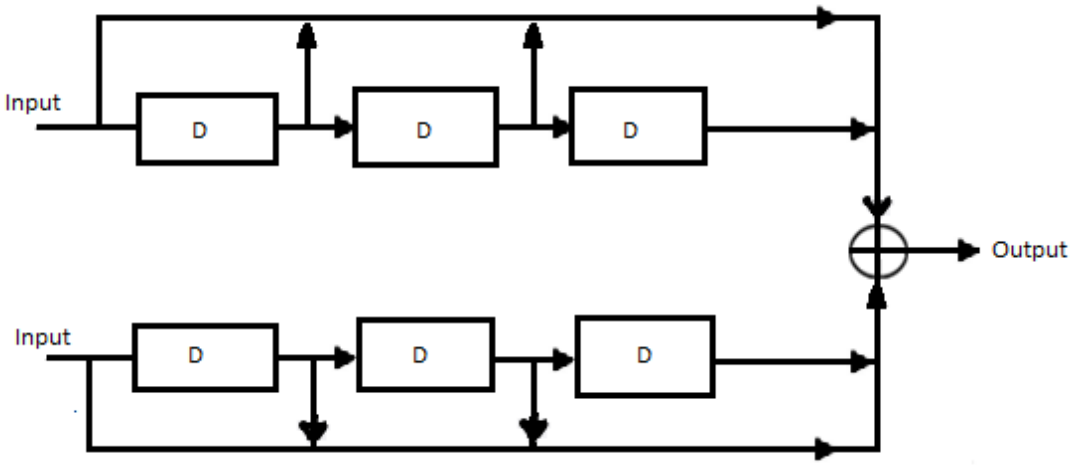

Figure 3.7 Syndrome Former for (13, 15)

equation is given as:

$$[H^{-1}]^T = [D + D^2 + D^3, 1 + D + D^2] \tag{3.24}$$

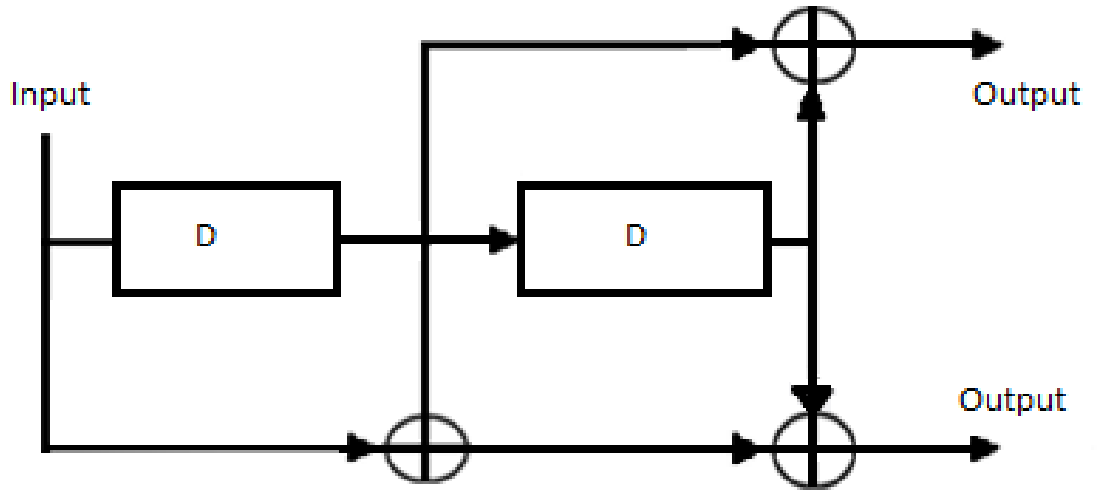

Figure 3.8 Inverse Syndrome Former for (13, 15)

3.4.4 Bit Error Probability 8 State Trellis

Like 4-state trellis, union bound is also applied for approximation for bit-error probability of 8 state trellis. The error probabilities of the bits previously encoded by $(H^{-1})^T$ are found by exploiting the Union bound. The equation for union bound is based similarly on the parameters that are: d_{free}, which is the code's minimum hamming distance, A_d which is code's weight distribution and lastly pd which is the likelihood of a wrongly chosen path at distance d. Summation of the error probabilities of the input bit sequence over all paths across distance d is given by union bound. The bit- error probabilities are calculated using the same equations given for 4 states trellis. For 8-state trellis, rate- 1/2 code, k=1, Bd_{free} = 1 and d_{free} = 5. Putting these values in equation (3.17), the bit-error probability $Pb_{s,f}$ for the encoded bit sequence is given by:

$$Pb_{s,f} \approx \frac{1}{2}(e^{\frac{S}{N}})^5 \tag{3.25}$$

3.4.5 The 16 State Trellis (19, 29) Code

The (23, 35) shaping code in octal refers to (19, 29) in decimal notation and forms a trellis with 16 states. The minimum hamming distance d(f) for this shaping code is 7. The encoder of this system has 4 memory units or shift registers and is shown in Fig. 3.9:

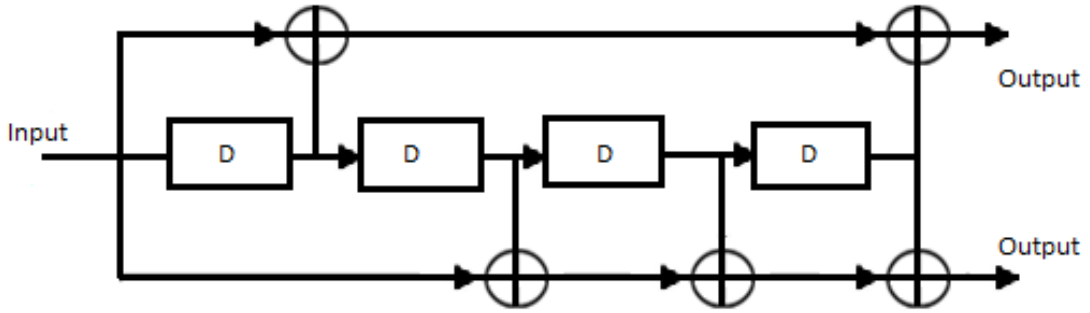

Figure 3.9 Convolution Code for (19, 29)

The Generator matrix of 16-states code is given as:

$$G = [1 + D + D^4, 1 + D^2 + D^3 + D^4] \tag{3.26}$$

The syndrome former or parity check matrix for (19, 29) is shown in Fig.3.10. Syndrome former equation, denoted by H, is written as:

$$[H^T] = [1 + D^2 + D^3 + D^4, 1 + D + D^4] \tag{3.27}$$

The [19, 29] syndrome former's left inverse is not distinctive. Syndrome former's left

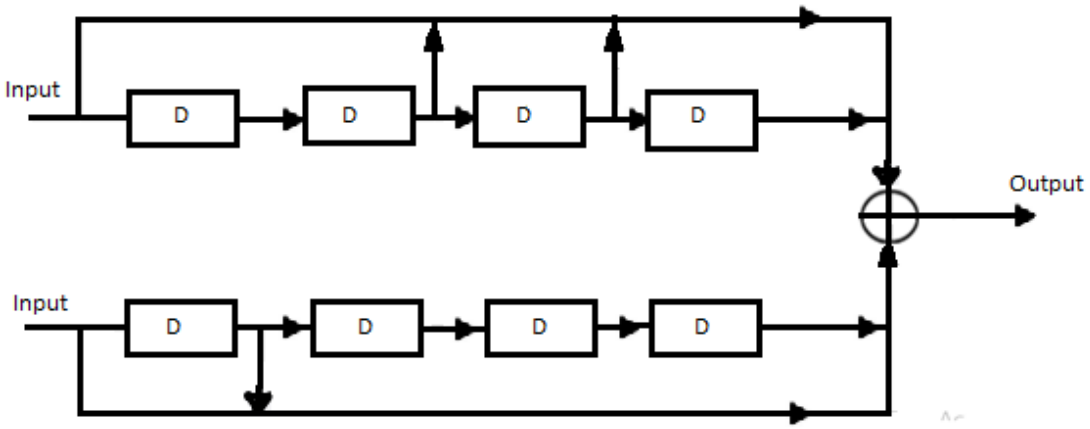

Figure 3.10 Syndrome Former for (19, 29)

inverse for (19,29) is given in Fig.3.11. One of the $(H^{-1})^T$ for 16-states trellis is given

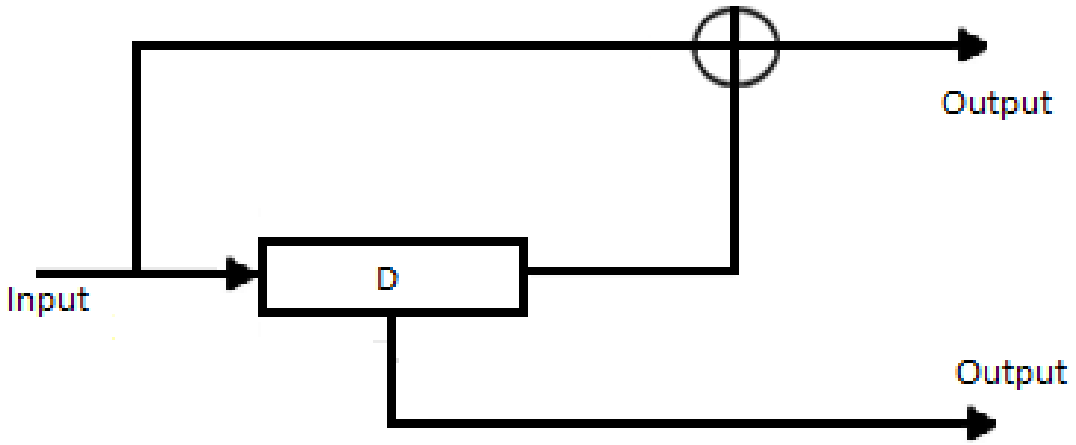

Figure 3.11 Inverse Syndrome Former for (19, 29)

as:

$$[H^{-1}]^T = [1 + D, D] \tag{3.28}$$

3.4.6 Bit Error Probability 16 State Trellis

Like 4-state and 8-state trellis, union bound is also applicable for approximation of bit-error probability of 16 state trellis. The error probabilities of the bits previously encoded by $(H^{-1})^T$ are found by exploiting the Union bound. The equation for union bound is based similarly on the parameters d_free, A_d and p_d. Summation of the error probabilities of the input bit sequence over all paths across distance d is given by union bound. The bit- error probabilities are calculated using the same equations as 8-state where k=1, $B_{d_{free}} = 1$ and $d_{free} = 3$. Thus, the bit-error probability $Pb_{s,f}$ of 16-state trellis is given by:

$$Pb_{s,f} \approx \frac{1}{2}(e^{\frac{S}{N}})^3 \tag{3.29}$$

Chapter 4

CONCATENATION OF OPTIMIZED LDPC WITH TS

In this chapter, we discuss the variable node degree distribution and its optimization algorithm. Along with this, we also discuss the LDPC code and its concatenation with trellis shaping. As the MSBs are passed through the inverse syndrome former, we also discuss briefly the multiple trellis depths used here.

4.1 Low Density Parity Check (LDPC) Codes

The low density parity check (LDPC) codes, initially designed by Gallager [51], are linear block codes with very high encoding complexity but they do have several advantages over turbo codes. To begin with the decoding of LDPC can be accomplished at relatively higher speeds. Secondly, decoders having the least complexity and that closely resemble belief propagation can be designed for these codes. Besides, the decoding of a correct code word is very much detectable. The encoding problem can somehow be limited by using a cascade of graphs instead of bipartite graphs.

Here we briefly describe some general properties of Low Density Parity Check codes. There characterization is done by a parity check matrix H_{n-k*n} where n shows code word length whereas the k shows input vector's length. The LPDC codes are characterized by bipartite graphs having check nodes and variable nodes. The H matrix of an LDPC code consists of a few non-zero values in each column. The condition given below, need to be fulfilled for a matrix to be low density. They are: $k >> w_r$ and $n >> w_c$. The LDPC code density is given by:

$$\xi_{ldpc} = w_r/n = w_c/k \tag{4.1}$$

4.1.1 Regular and Irregular LDPC Codes

LDPC code of length n is represented by an ordered pair (n, wc, wr). Each information bit is connected with wc parity checks whereas information bits are connected to wr parity check bits [52]. The total number of edges attached to a node is its degree. The regular and irregular LDPC codes are differentiated by the degree of nodes.

If all the variable nodes have the same degree and the check nodes have another common degree, the code is referred to as a regular LDPC code [83]. Fig.4.1 shows regular LDPC code. As we can see that there are 4 check nodes and 8 variable nodes. The number of edges connected to all check nodes is 4. Thus the degree of all check nodes is same that is 4. Similarly, degree of all variable nodes is same that is 2.

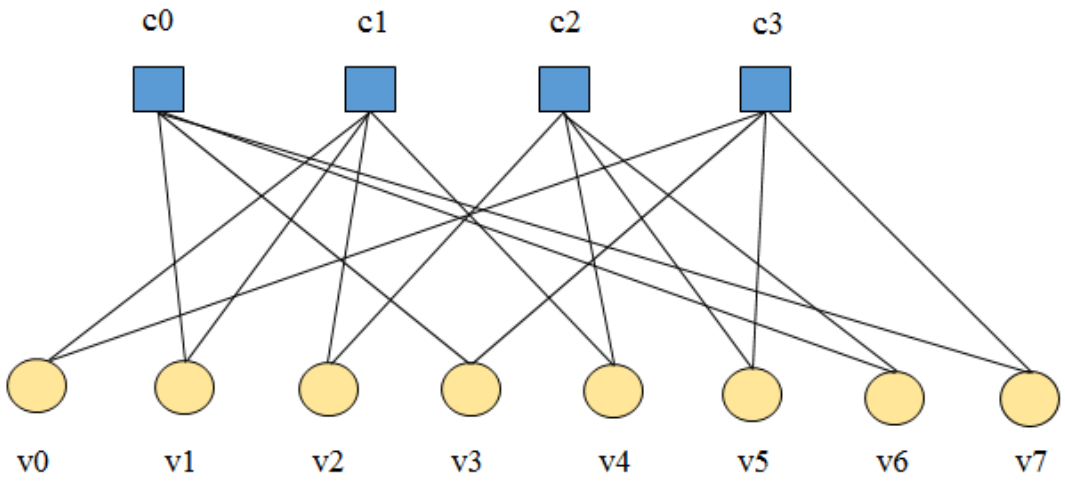

Figure 4.1 Regular LDPC Code

In irregular LDPC codes [53], the degree of the variable nodes are different from one another and degree of variable nodes is also different [84]. Fig.4.2 represents irregular LDPC code. As we can see that there are 3 check nodes and 6 variable nodes. Degree of the check nodes is not same. One check node has 2 edges and the remaining check nodes have 3 edges. Similarly, degree of variable nodes is also not same. 2 variable nodes have 2 edges and remaining variable nodes have 1 edge.

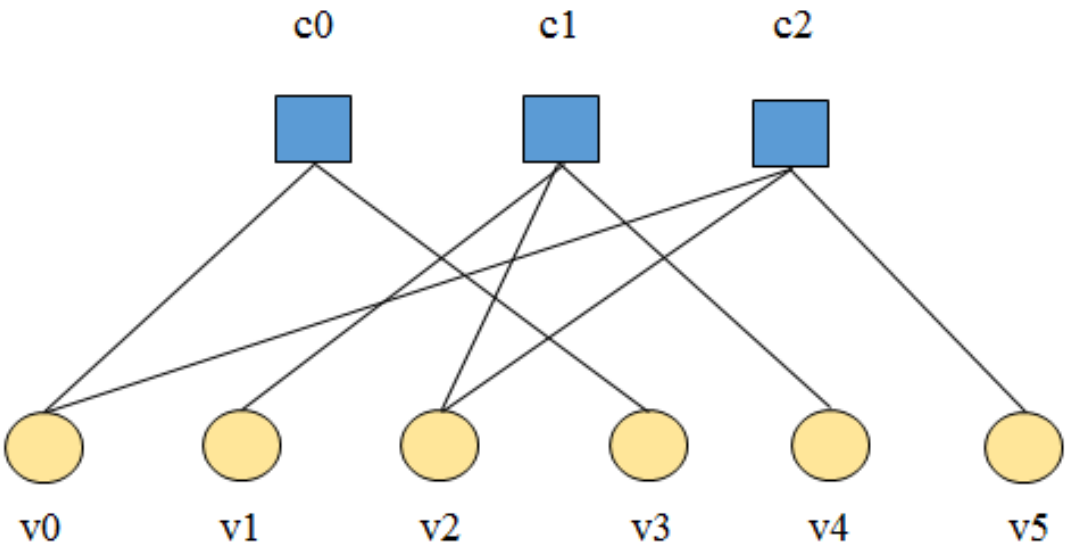

Figure 4.2 Irregular LDPC Code

4.2 Optimisation of Variable-Node Degree Distribution

For optimizing the variable node degree distribution for LDPC, let us consider an Unequal Error protection (UEP) LDPC code [54] with a code word length N. The different bit error probabilities of each bit of a QAM symbol are used for the optimization [55]. Let us suppose that Nm represents the total number of modulation classes. The vector β_i shows the number of bits in the respective modulation class where β_i is the proportion of bits assigned to each ith modulation class. The vector λ is the combined degree distribution of all the modulation classes. For the construction of an irregular LDPC codes, the check-node degree distribution is also required. The check node degree distribution is given by:

$$\rho = [\rho_2, \rho_3, ..., \rho_{dc}] \tag{4.2}$$

The distribution of variable degree of node is optimized with the maximum degree i.e. dvmax despite all the constraints to have a high code rate [56]. The process of optimization is carried out in such a way as to maximize the code rate. For the algorithm, the following values must be known: The requisite code rate R, Variance σ^2, variable node degree $d_{v_{max}}$, check node distribution ρ, along with the bits proportion in each class of modulation β. The algorithm involves the calculation of proportion

distribution constraint for optimization, given as:

$$\sum_{j=1}^{N_m} \sum_{i=2}^{d_{vmax}} \lambda_{M_{j,i}} = 1 \tag{4.3}$$

Its convergence and stability constraints are given respectively as:

$$F(\lambda, \rho, \sigma^2, x) > x \tag{4.4}$$

$$\sum_{j=1}^{N_m} \lambda_{M_{j,2}} < [\sum_{j=1}^{N_m} \beta_j e^{-1/2\sigma_j^2} . \sum_{i=2}^{d_{vmax}} \rho_m(m-1)]^{-1} \tag{4.5}$$

4.3 Concatenation of LDPC Code with TS

Soft decision decoding involving the algorithm of BCJR, was proposed by authors in [57, 58]. This decoding was based on the shaping code and inverse syndrome former. Authors concatenated a regular code of LDPC with TS for PAR reduction to enhance the BER rate. Higher QAM modulations were used at each OFDM tone. For constellations of higher order, QAM-symbol bits possess different probabilities of error. These irregularities in probabilities of error in QAM symbols, gives rise to the chance of implementation of LDPC codes. This motivation lead to design an irregular LDPC code concatenated with TS. The concatenation was based on the differences in the error probabilities of the single bits in QAM constellation [59].

4.3.1 System Model for Concatenation of LDPC Code

Besides PAPR Reduction, we will also optimize the degree distribution of variable node by exploiting the individual bit error probability of higher order QAM constellation for LDPC codes. U represents the input bit stream which is encoded in beginning using an irregular LDPC code. The encoded bits are based on different probabilities of error. These bits are allotted to different modulation classes of QAM symbol [60]. For irregular LDPC code implementation, we have to exploit the irregularities in the QAM symbol. Block diagram of LDPC code, concatenated with TS, is given in Fig. 4.3. Encoding of the input bit stream 'u' is done with irregular LDPC code. Individual

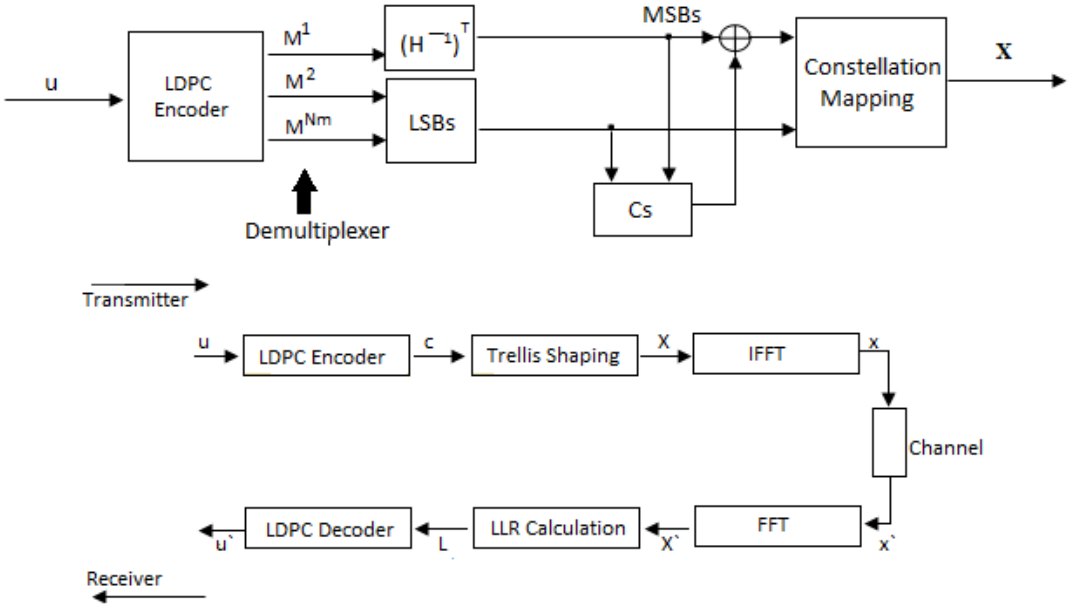

Figure 4.3 Block diagram of LDPC code concatenated with Trellis Shaping

bits are present inside the M-ary QAM symbol. These bits are used for LDPC code optimization i.e the bit error probabilities of each bit are exploited for optimization. As its obvious from our previous discussion that irregular LDPC codes outperform the regular LDPC codes. Herein, we consider a regular (3, 21) LDPC code. This has the same rate of code like irregular LDPC codes. For the variable node degree optimization, we exploited the error probabilities calculated for different shaping codes using union bound. Results for BER plot comparison for regular and irregular LDPC codes are shown in next chapter.

4.4 Bahl-Cocke-Jelinek-Raviv (BCJR)

The inclusion of Bahl-Cocke-Jelinek-Raviv (BCJR) algorithm into the decoding process is to enhance the system performance. Previously, hard decision decoding was used at the receiver for decoding the information bit sequence. This hard decision decoding was carried out on the channel outputs in Trellis shaping as is evident from [61]. However, combining soft decision decoding to BCJR algorithm shows significant performance improvement. Therefore, we have inculcated soft decision decoding to BCJR algorithm which yields the Log-Likelihood ratios (LLRs) of the sequence of shaping bits. Here

Let's suppose that the QAM symbol selected by Trellis shaping is $X = [X_n], n = 1, 2, ...N,$. IFFT is performed to receive x which is then transmitted. At the DFT domain nth data symbol estimated at the receiver is given by following equation where, Y_n gives the nth tone of the frame in OFDM:

$$Y_n(Output) = X_n(Input) + w_n(Noise) \tag{4.6}$$

At the transmitter, LSBs are mapped directly without any pre-processing. The equation below, gives the LLRs for the LSBs, yielded by channel output. This equation shows that the ith received bit's probability density function (pdf) is based on the nth transmitted symbol.

$$\mathscr{L}^n_{LS\,Bs} = ln\frac{p(c_{n,1} = 0|X)}{p(c_{n,1} = 1|X)} \tag{4.7}$$

4.4.1 Metric Design for BCJR Algorithm

A combined Trellis system based on generator matrix of the shaping code Cs and $(H^{-1})^T$ i.e left inverse of syndrome former is incorporated to get soft outputs for the MSBs. The LLRs are then determined by using BCJR based on this combined trellis. The complete amount of states in combined trellis is given by:

$$N_{s_{ct}} = N_{s_{cs}} N_{sH} \tag{4.8}$$

The number of branches preceding from each state of combined trellis is 2n (n is the shaping code's total number of output bits). The forward and backward recursion, respectively given below, are computed before the calculation of soft output of the BCJR.

$$\alpha_n(l) = \sum_{i=1}^{N_{s_{ct}}} \alpha_{n-1}(l'_i)\gamma_{n-1}(l'_i, l) \tag{4.9}$$

$$\beta_n(l') = \sum_{i=1}^{N_{s_{ct}}} \beta_{n+1}(l_i)\gamma_n(l', l_i) \tag{4.10}$$

State transition probabilities are also computed before the calculation of soft output of the BCJR. State transition probabilities are calculated as:

$$\gamma_n(l', l) = \Pi_{j=1}^{2-1} p_{n,j}(l', l|X_n) \tag{4.11}$$

In case of no connection between l0 and l then n(l0, l) is equal to 0. After getting all the above data i.e. forward and backward recursions and state transitions, the likelihood for jth received bit of the MSBs is computed by:

$$p(z_n'^{\,j} = b, X) = \sum_{\zeta \epsilon \Upsilon(b)} \alpha_n(l')\gamma_n(l', l)\beta_{n+1}(l) \tag{4.12}$$

where $z_n'^{\,j}$ n is the received jth symbol belonging to the MSBs. Finally, the LLRs are calculated by:

$$\mathscr{L}_{MSBs}^{n} = ln\frac{p(z_n'^{\,j} = 0|X)}{p(z_n'^{\,j} = 1|X)} = ln\frac{p(z_n'^{\,j} = 0, X)}{p(z_n'^{\,j} = 1, X)} \tag{4.13}$$

The LLRs of both MSBs and LSBs are fed into LDPC decoder to retrieve information for the entire bit sequence u.

Chapter 5

RESULTS AND DISCUSSIONS

In this chapter, we will discuss simulation results for different trellis depths. We will also compare results for different window sizes and show which has better performance in terms of gain. We will also plot FER curves for ACE based TS. Results for LDPC code concatenated with TS, will also be discussed here.

5.1 Simulation Results for Different Trellis Depths

The simulation results of varying depths trellis shaping codes are now discussed. All the simulations are performed in MATLAB 2018a. This simulation is done for 256-QAM, with 128 sub-carriers and the simulation counter is set to 1000. The window size is 32. Fig.5.1, Fig.5.2 and Fig.5.3 show CCDF vs PAPR plot for 4-state, 8-state and 16-state. We can see from the results that 16-state Trellis has better PAPR gain improvement as compared to other states. Similarly 8-state Trellis has better results than 4-state Trellis. It is evident from the plot that increasing the trellis depth of the shaping codes, PAPR reduction is improved which shows that higher gains can be obtained using shaping codes of higher states. An increased gain of almost 2.5-2.8dB can be seen for different state shaping codes of ACE based TS.

5.1.1 4-state Trellis Depth

Fig.5.1 is for 4-state Trellis in which the right most curve shows gain without any PAPR. The middle curve shown gain for PAPR Reduction using TS. The left most curve shows gain for PAPR Reduction with ACE based TS which is about 6.4dB. We can see that gain is improved using combined PAPR technique of ACE based TS as compared to only TS.

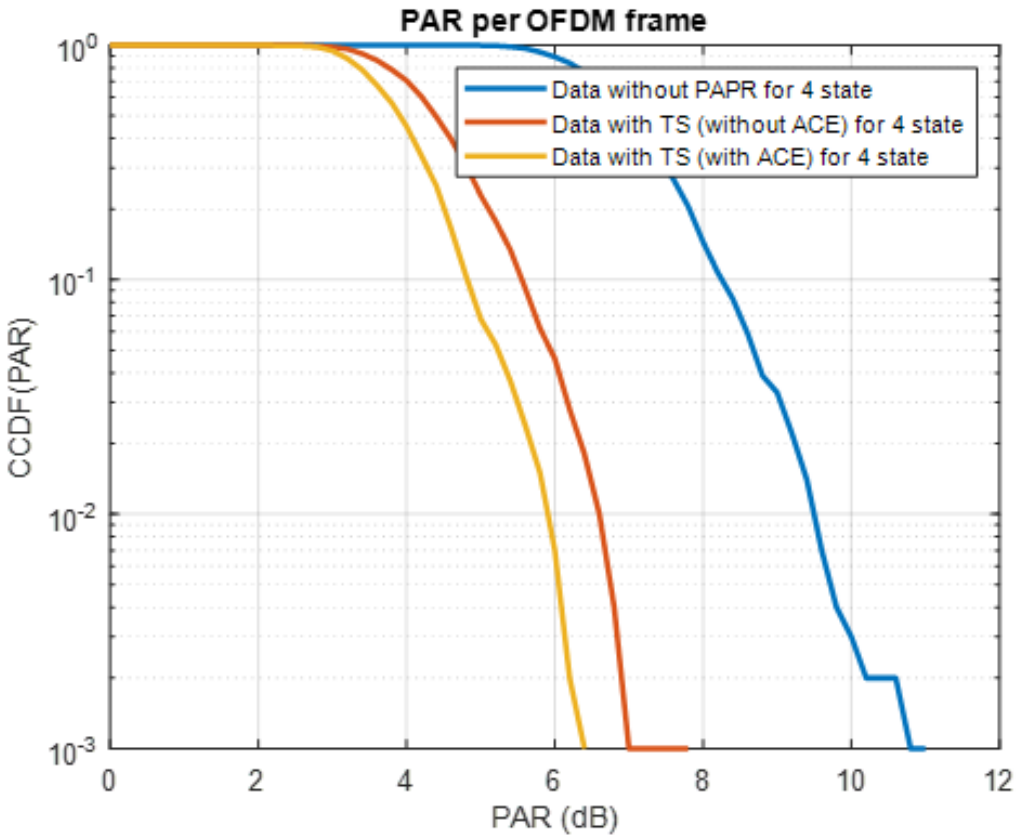

Figure 5.1 PAPR curve for 4-state Trellis

5.1.2 8-state Trellis Depth

Fig. 5.2 is for 8-state Trellis in which the right most curve shows gain without any PAPR. The middle curve shown gain for PAPR Reduction using TS which is about 7.3dB. The left most curve shows gain for PAPR Reduction with ACE based TS which is about 6.3dB. We can see the gain improvement gain using combined PAPR technique of ACE based TS as compared to only TS.

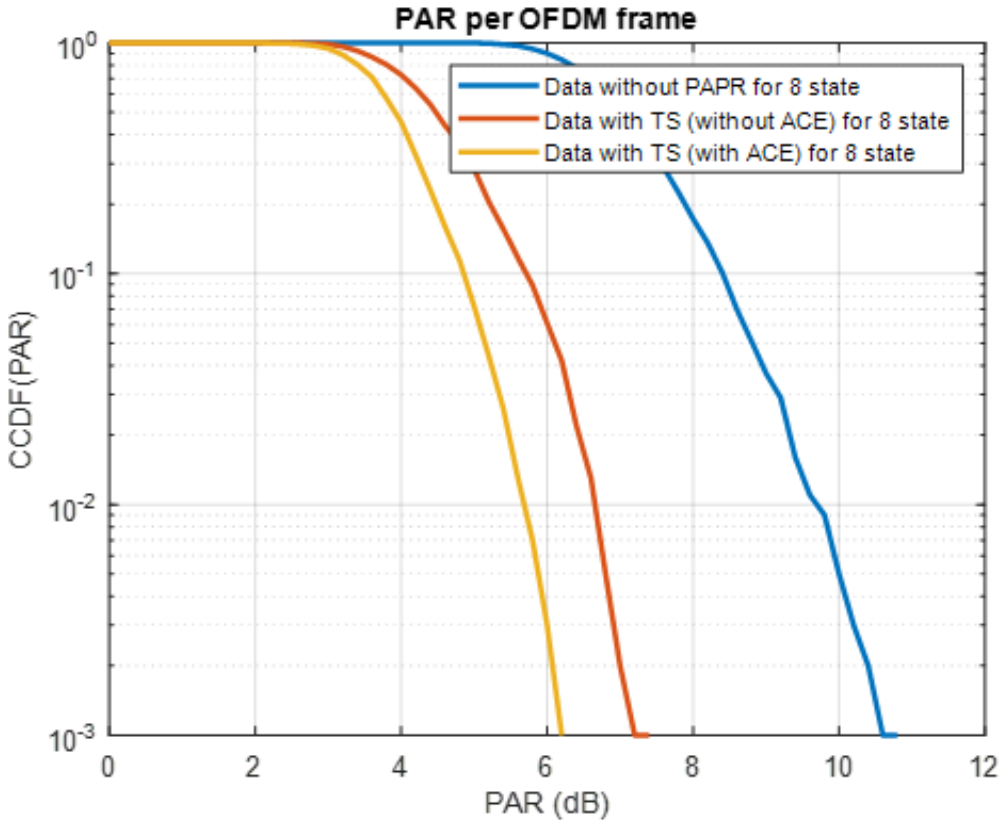

Figure 5.2 PAPR curve for 8-state Trellis

5.1.3 16-state Trellis Depth

Fig.5.3 is for 16-state Trellis in which the right most curve shows gain without any PAPR. The middle curve shown gain for PAPR Reduction using TS which is about 7.2dB. The left most curve shows gain for PAPR Reduction with ACE based TS which is about 6.1dB. We can clearly see that gain is improved using combined PAPR technique of ACE based TS as compared to only TS.

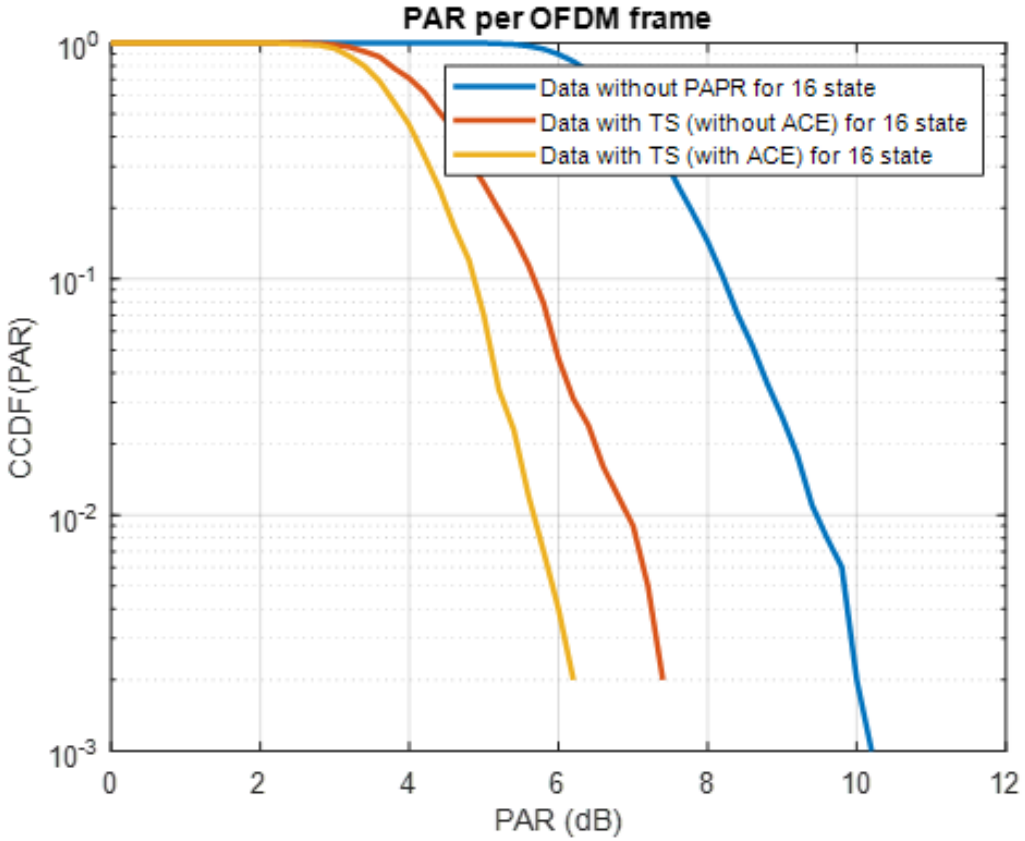

Figure 5.3 PAPR curve for 16-state Trellis

5.2 Simulation Results for ACE based TS for Same Window Sizes

In Fig.5.4, Fig.5.5 and Fig.5.6, PAPR curves are plotted for ACE based TS for same window sizes. These curves are plotted for 4, 8 and 16 state for 256-QAM. We can see from the results that 16-state Trellis has better PAPR gain improvement as compared to other states in case when window size is kept same.

5.2.1 Window Size 32

Fig.5.4 shows ACE based TS curve for same window size of 32. The right most curve shows gain for 4-state trellis without PAPR Reduction. The red curve shows gain for 4-state with TS only. The yellow curve shows gain for 4-state ACE based trellis with 32 window size. The purple curve shows gain for 16-state ACE based trellis with 32 window size. By comparing these graphs, we can see that 16 state trellis with 32 window size has better results than the rest states. This shows that increasing the trellis state will provide us better gain for PAPR Reduction.

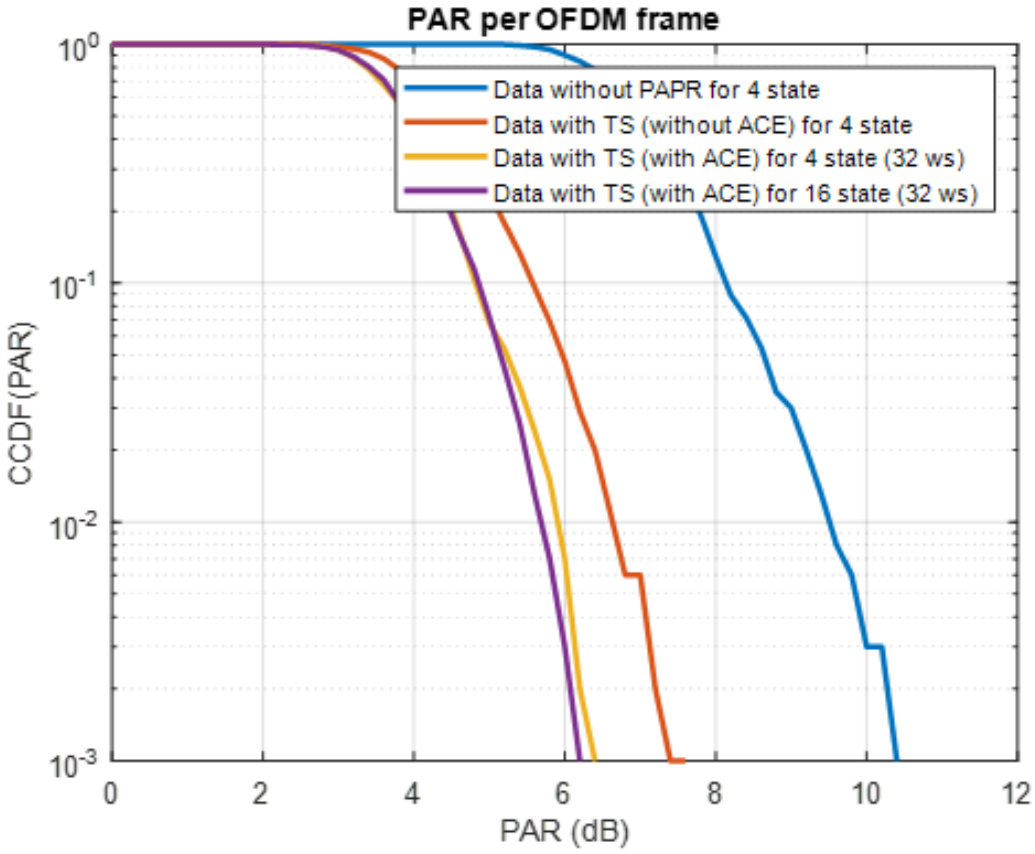

Figure 5.4 PAPR curve for window size 32

5.2.2 Window Size 64

Fig.5.5 shows ACE based TS curve for same window size of 64. The right most curve shows gain for 4-state trellis without PAPR Reduction. The red curve shows gain for 4-state with TS only. The yellow curve shows gain for 4-state ACE based trellis with 64 window size. The purple curve shows gain for 16-state ACE based trellis with 64 window size. By comparing these graphs, we can see that 16 state trellis with 64 window size has better results than the rest states.

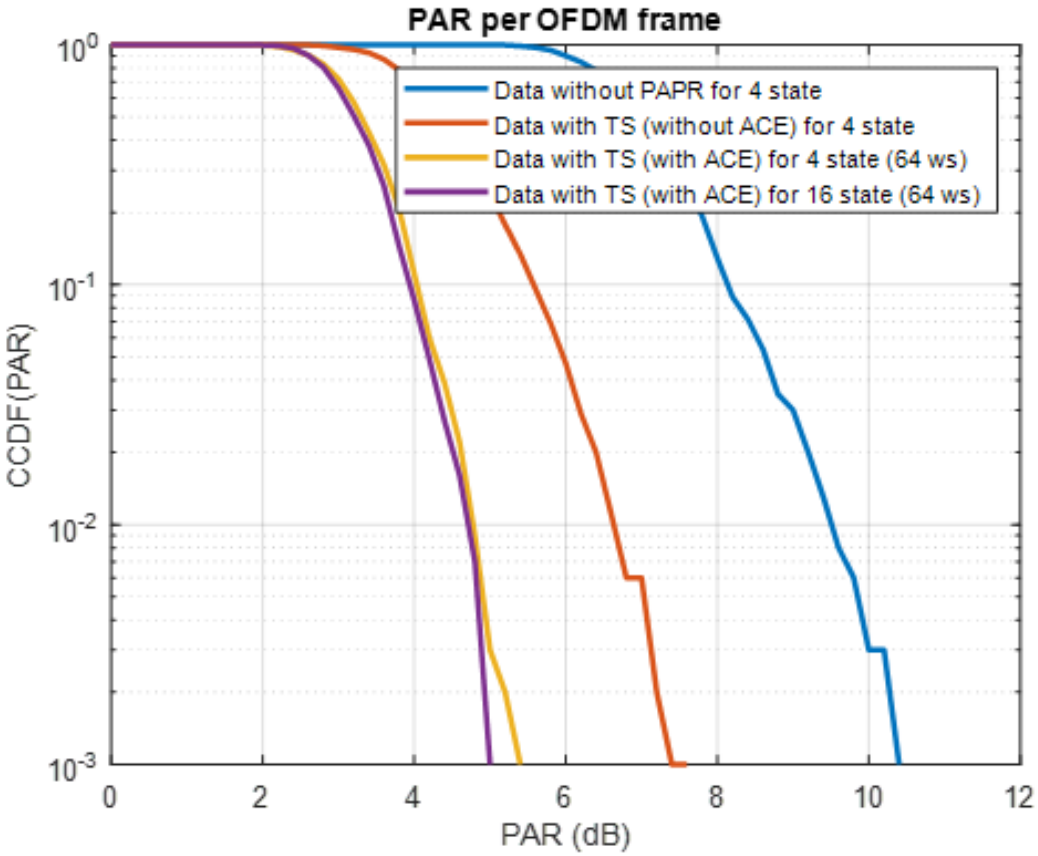

Figure 5.5 PAPR curve for window size 64

5.2.3 Window Size 128

Fig.5.6 shows ACE based TS curve for same window size of 128. The right most curve shows gain for 4-state trellis without PAPR Reduction. The red curve shows gain for 4-state with TS only. The yellow curve shows gain for 4-state ACE based trellis with 128 window size. The purple curve shows gain for 8-state ACE based trellis with 128 window size. The green curve shows gain for 16-state ACE based trellis with 128 window size.

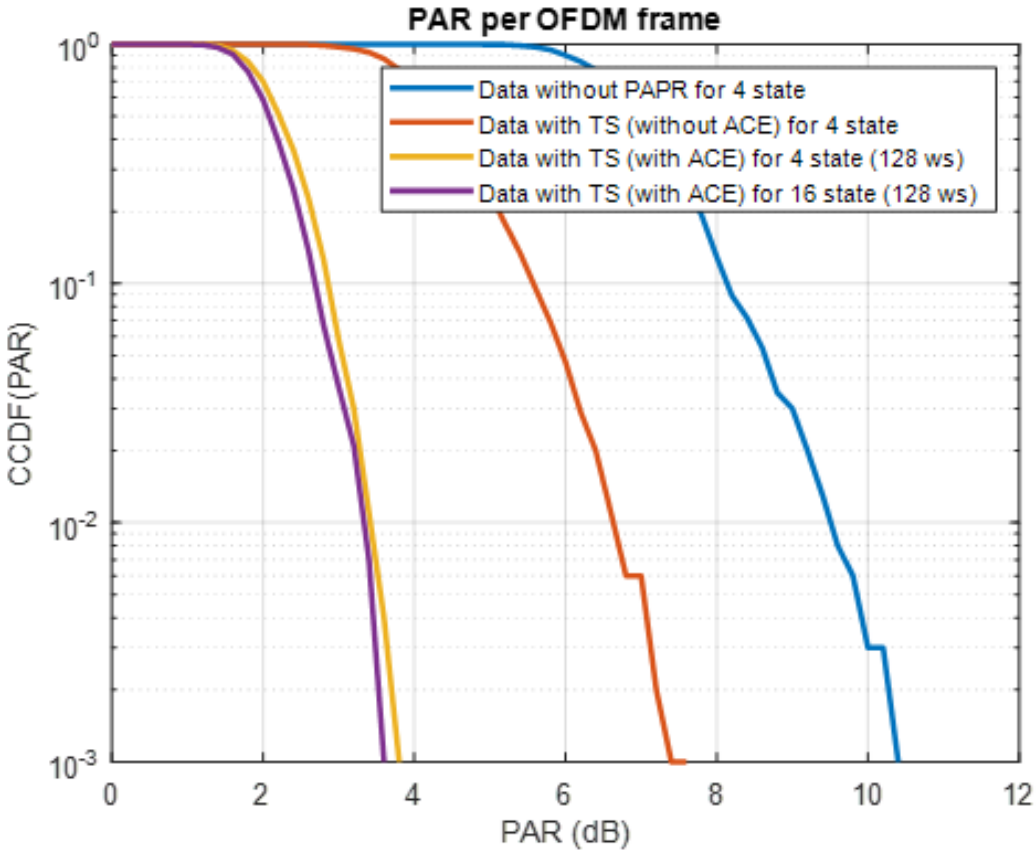

Figure 5.6 PAPR curve for window size 128

5.3 Simulation Results for ACE based TS for Different Window Sizes (Same Complexity)

Fig.5.7 shows ACE based TS curve for different window size. Curves for 128 window size for 4-state, 64 window size for 8-state and 32 window size for 16-state are showing same complexity. The right most curve shows gain for 4-state trellis without PAPR Reduction. The red curve shows gain for 4-state with TS only. The green curve shows gain for 16-state ACE based trellis with 32 window size. The purple curve shows gain for 8-state ACE based trellis with 64 window size. The yellow curve shows gain for 4-state ACE based trellis with 128 window size. By comparing these graphs, we can see that 4 state trellis with 128 window size, has better results than the rest states. This shows that increasing the window size will provide us better gain for PAPR Reduction.

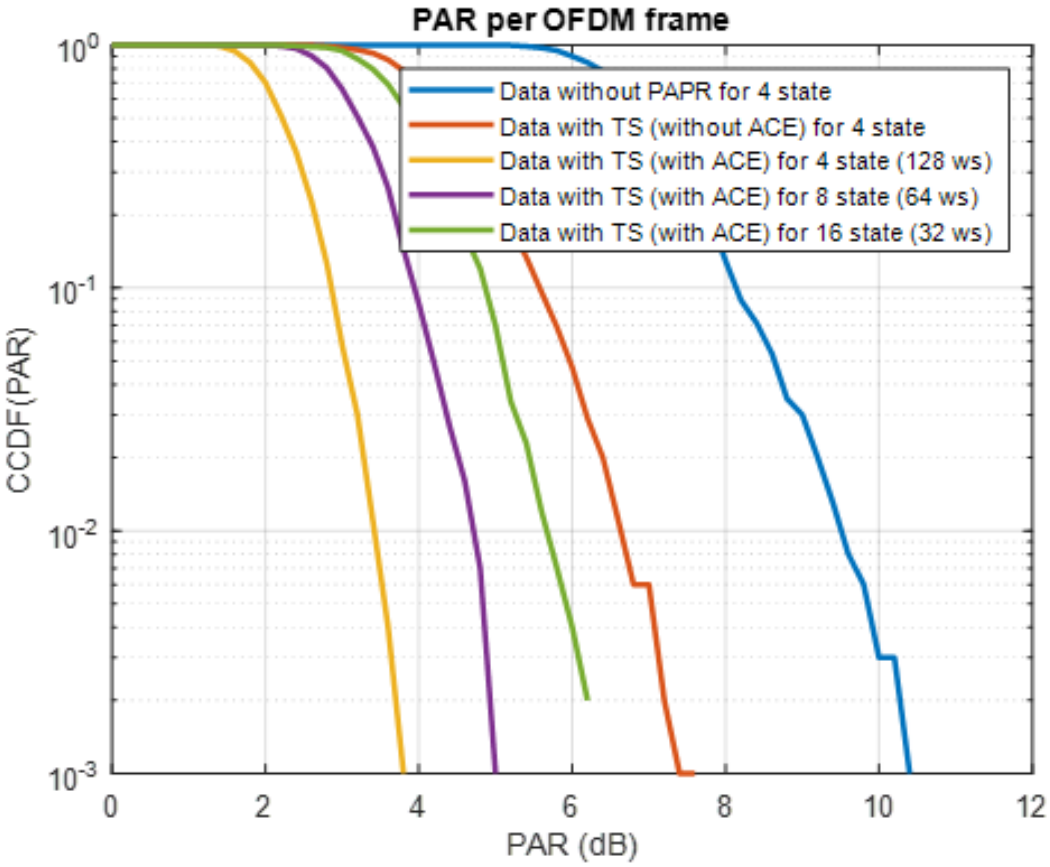

Figure 5.7 PAPR curve for same complexity

5.4 Simulation Results for FER Plot

Results were generated for FER curves of shaping codes with various depths with hard decision decoding using the syndrome former. Fig.5.8 shows FER vs Eb/No (Energy Per Bit to Noise Density Ratio) plot for 16-QAM for 4-state and 16-state. Fig.5.8 shows FER curve for TS (without ACE) and TS (with ACE) for 32 window size. The blue curve shows frame error rate plot for 4-state trellis using PAPR Reduction technique of TS without ACE. The red curve shows FER plot for 4-state with ACE based TS. The yellow curve shows frame error rate plot for 16-state trellis using PAPR Reduction technique of TS without ACE. The purple curve shows FER plot for 16-state with ACE based TS. By comparing these graphs, we can clearly see that when we use combine technique of ACE bases TS, we get better frame error performance. We can see from the results that 16-state Trellis has better FER performance as compared to 4-states.

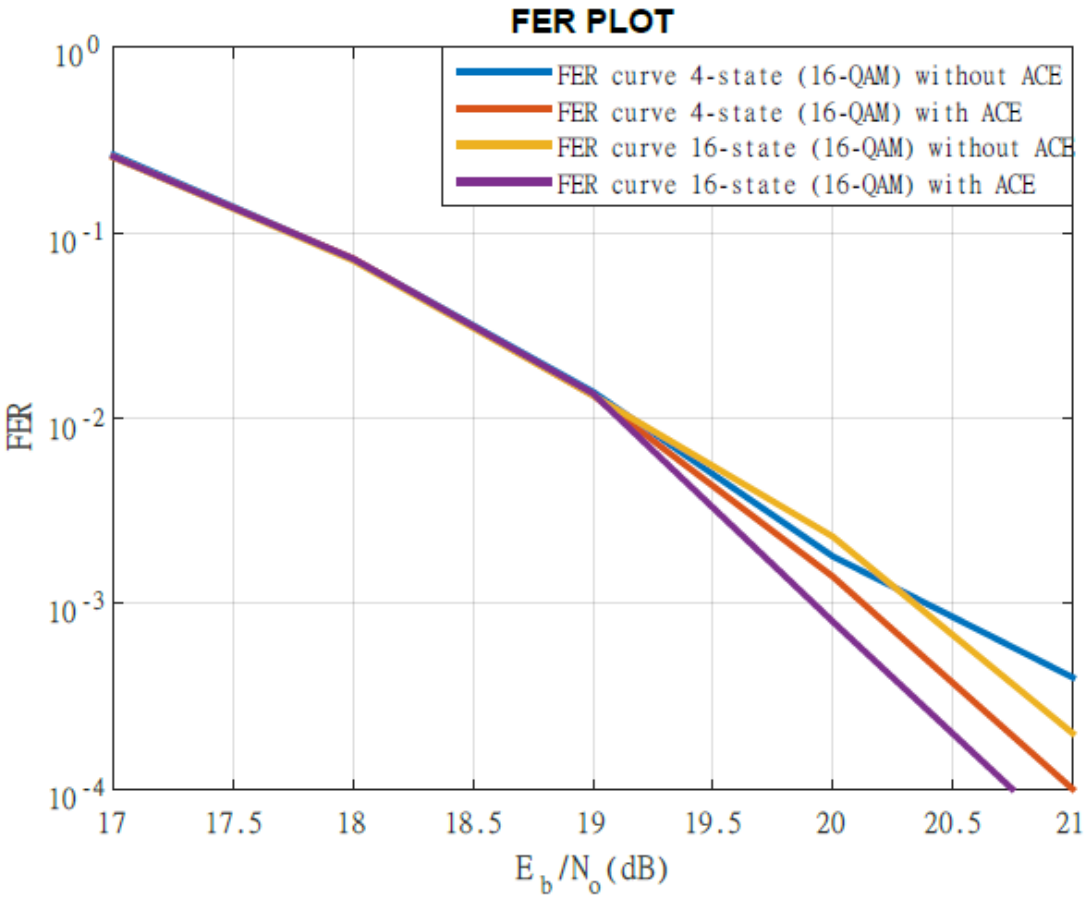

Figure 5.8 FER plot for 4-state and 16-state

5.5 LDPC Code Concatenation With TS

Single-input Single-output (SISO) OFDM system is considered here which is appended to a rate - k/n LDPC code. For simulation results, a 256-QAM constellation is considered with Gray mapping. The LDPC codes used are both regular and irregular to compare the spectral efficiencies. Here we have considered 256 QAM modulation for an OFDM frame of 128 subcarriers. As we already know that each 256 QAM symbol comprises of 8 bits per symbol, the bits required to match one OFDM frame are $8 \times 128 = 1024$ bits [95]. One redundant bit per symbol is added by the Trellis shaping block appended with LDPC code. Therefore, matching the size of LDPC with one OFDM frame, requires LDPC code to be picked-out as 896 (896 + 128 =1024). This makes the system's collective code rate equal to 3/4. Belief Propagation (BP) is used with maximum iterations 30 for LDPC code word decoding. For regular and irregular LDPC [96], the maximum iterations limit is 30. For comparison of our results with system without Trellis shaping, the code word length is set to 1024 and code rate is 3/4. Fig.5.9 shows the BER curves for regular and irregular LDPC codes using 4-state and 8-state trellis shaping. It can be seen that the system performance improves using shaping codes of larger depths. The system performance is improved by 0.2 dB using 8-states shaping as compared to the one using 4-states shaping code.

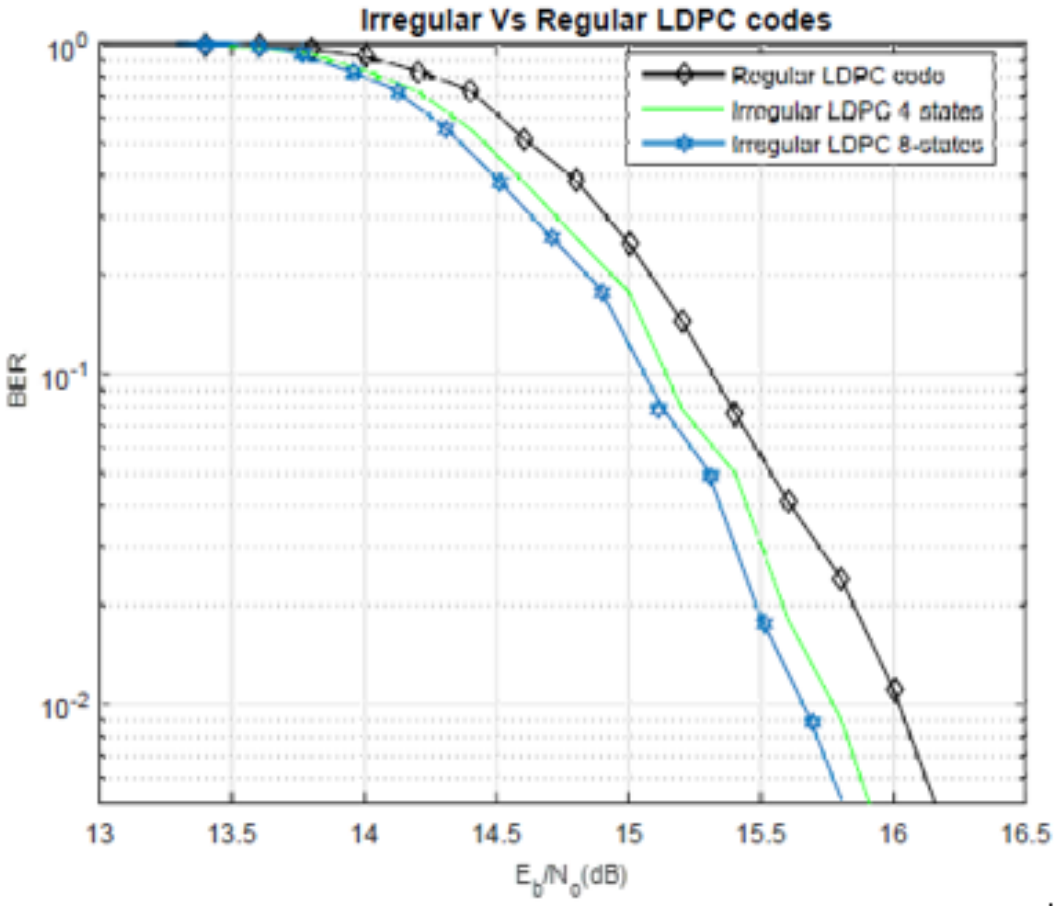

Figure 5.9 BER plot for Regular and Irregular LDPC 896

Chapter 6

CONCLUSION

6.1 Conclusion

Herein, using trellis shaping combined with active constellation extension for PAPR reduction in SISO systems. We have used shaping codes of various trellis depths. The results of simulation shows that the system performance and gain can be enhanced in terms of PAPR, using shaping codes of larger trellis depths. We have achieved an increased gain of almost 2.5dB using ACE based TS as compared to TS only. However, we get the gain at the cost of a slight increase in the system computational complexity. Moreover, FER curves are also evaluated for different shaping codes using TS and ACE based TS in this research. The results show that we have achieved almost 0.2-0.3 dB more gain for FER plot when we use ACE based TS. We have also found out the error probabilities of various trellis depths of shaping codes using union bounds. To improve the performance of system in terms of BER, we have combined the irregular LDPC code with TS using different trellis depths. For irregular LDPC codes, the variable node degree distribution was optimized by exploiting the error probabilities of individual bits that are present inside the M-ary QAM symbol. It can be seen that the results for larger depth trellis shaping codes performs better than the 4-state trellis shaping code.

6.2 Future Work

PAPR Reduction using ACE based TS can be extended in future for Non-orthogonal multiple access OFDM systems (NOMA-OFDM). NOMA technique can satisfy the performance requirements for fifth-generation (5G) communications systems. This technique outperforms the traditional multiple access schemes in many aspects. It uses superposition coding (SC) to share the available resources among the users and adopts successive interference cancelation (SIC) for multiuser detection (MUD). NOMA technique can increase the number of users, improve spectrum efficiency, ensure massive connectivity, high performance, and low latency.

BIBLIOGRAPHY

[1] J. Chuang and N. Sollenberger, "Beyond 3g: wideband wireless data access based on ofdm and dynamic packet assignment," *IEEE Communications Magazine*, vol. 38, no. 7, pp. 78–87, 2000.

[2] A. Jayalath and C. Tellambura, "Peak-to-average power ratio reduction of an ofdm signal using data permutation with embedded side information," in *ISCAS 2001. The 2001 IEEE International Symposium on Circuits and Systems (Cat. No.01CH37196)*, vol. 4, 2001, pp. 562–565 vol. 4.

[3] B. Saltzberg, "Performance of an efficient parallel data transmission system," *IEEE Transactions on Communication Technology*, vol. 15, no. 6, pp. 805–811, 1967.

[4] R. R. Mosier and R. G. Clabaugh, "Kineplex, a bandwidth-efficient binary transmission system," *Transactions of the American Institute of Electrical Engineers, Part I: Communication and Electronics*, vol. 76, no. 6, pp. 723–728, 1958.

[5] M. Zimmerman and A. Kirsch, "The an/gsc-10 (kathryn) variable rate data modem for hf radio," *IEEE Transactions on Communication Technology*, vol. 15, no. 2, pp. 197–204, 1967.

[6] S. Weinstein and P. Ebert, "Data transmission by frequency-division multiplexing using the discrete fourier transform," *IEEE Transactions on Communication Technology*, vol. 19, no. 5, pp. 628–634, 1971.

[7] A. Peled and A. Ruiz, "Frequency domain data transmission using reduced computational complexity algorithms," in *ICASSP '80. IEEE International Conference on Acoustics, Speech, and Signal Processing*, vol. 5, 1980, pp. 964–967.

[8] Y. Wu and W. Zou, "Orthogonal frequency division multiplexing: a multi-carrier modulation scheme," *IEEE Transactions on Consumer Electronics*, vol. 41, no. 3, pp. 392–399, 1995.

[9] A. Petropulu, R. Zhang, and R. Lin, "Blind ofdm channel estimation through simple linear precoding," *IEEE Transactions on Wireless Communications*, vol. 3, no. 2, pp. 647–655, 2004.

[10] ——, "Blind ofdm channel estimation through simple linear precoding," *IEEE Transactions on Wireless Communications*, vol. 3, no. 2, pp. 647–655, 2004.

[11] T. Hwang, C. Yang, G. Wu, S. Li, and G. Ye Li, "Ofdm and its wireless applications: A survey," *IEEE Transactions on Vehicular Technology*, vol. 58, no. 4, pp. 1673–1694, 2009.

[12] S. C and J. Sandeep, "A review of channel estimation mechanisms in wireless communication networks," in *2021 5th International Conference on Electronics, Communication and Aerospace Technology (ICECA)*, 2021, pp. 603–608.

[13] M. Saeed, B. Ali, and M. Habaebi, "Performance evaluation of ofdm schemes over multipath fading channels," in *9th Asia-Pacific Conference on Communications (IEEE Cat. No.03EX732)*, vol. 1, 2003, pp. 415–419 Vol.1.

[14] T. Jiang and Y. Wu, "An overview: Peak-to-average power ratio reduction techniques for ofdm signals," *IEEE Transactions on Broadcasting*, vol. 54, no. 2, pp. 257–268, 2008.

[15] J. G. Andrews, S. Buzzi, W. Choi, S. V. Hanly, A. Lozano, A. C. K. Soong, and J. C. Zhang, "What will 5g be?" *IEEE Journal on Selected Areas in Communications*, vol. 32, no. 6, pp. 1065–1082, 2014.

[16] R. Chang and R. Gibby, "A theoretical study of performance of an orthogonal multiplexing data transmission scheme," *IEEE Transactions on Communication Technology*, vol. 16, no. 4, pp. 529–540, 1968.

[17] Y. Rahmatallah and S. Mohan, "Peak-to-average power ratio reduction in ofdm systems: A survey and taxonomy," *IEEE Communications Surveys Tutorials*, vol. 15, no. 4, pp. 1567–1592, 2013.

[18] X. Li and L. Cimini, "Effects of clipping and filtering on the performance of ofdm," in *1997 IEEE 47th Vehicular Technology Conference. Technology in Motion*, vol. 3, 1997, pp. 1634–1638 vol.3.

[19] A. Gatherer, M. Polley, and A. Redfern, "Par reduction for dmt systems with unloaded subchannels," in *Conference Record of the Thirty-Sixth Asilomar Conference on Signals, Systems and Computers, 2002.*, vol. 2, 2002, pp. 1847–1851 vol.2.

[20] J. Armstrong, "New ofdm peak-to-average power reduction scheme," in *IEEE VTS 53rd Vehicular Technology Conference, Spring 2001. Proceedings (Cat. No.01CH37202)*, vol. 1, 2001, pp. 756–760 vol.1.

[21] K. Anoh, C. Tanriover, and B. Adebisi, "On the optimization of iterative clipping and filtering for papr reduction in ofdm systems," *IEEE Access*, vol. 5, pp. 12 004–12 013, 2017.

[22] H. Breiling, S. Muller-Weinfurtner, and J. Huber, "Slm peak-power reduction without explicit side information," *IEEE Communications Letters*, vol. 5, no. 6, pp. 239–241, 2001.

[23] Y.-L. Lee, Y.-H. You, W.-G. Jeon, J.-H. Paik, and H.-K. Song, "Peak-to-average power ratio in mimo-ofdm systems using selective mapping," *IEEE Communications Letters*, vol. 7, no. 12, pp. 575–577, 2003.

[24] C. Siegl and R. F. Fischer, "Peak-to-average power ratio reduction in multi-user ofdm," in *2007 IEEE International Symposium on Information Theory*, 2007, pp. 2746–2750.

[25] C. Siegl and R. F. H. Fischer, "Asymptotic performance analysis and successive selected mapping for par reduction in ofdm," *IEEE Transactions on Signal Processing*, vol. 58, no. 6, pp. 3228–3237, 2010.

[26] C.-L. Wang and Y. Ouyang, "Low-complexity selected mapping schemes for peak-to-average power ratio reduction in ofdm systems," *IEEE Transactions on Signal Processing*, vol. 53, no. 12, pp. 4652–4660, 2005.

[27] S. Muller and J. Huber, "A comparison of peak power reduction schemes for ofdm," in *GLOBECOM 97. IEEE Global Telecommunications Conference. Conference Record*, vol. 1, 1997, pp. 1–5 vol.1.

[28] A. Alavi, C. Tellambura, and I. Fair, "Papr reduction of ofdm signals using partial transmit sequence: an optimal approach using sphere decoding," *IEEE Communications Letters*, vol. 9, no. 11, pp. 982–984, 2005.

[29] S. H. Han and J. H. Lee, "Papr reduction of ofdm signals using a reduced complexity pts technique," *IEEE Signal Processing Letters*, vol. 11, no. 11, pp. 887–890, 2004.

[30] ——, "Papr reduction of ofdm signals using a reduced complexity pts technique," *IEEE Signal Processing Letters*, vol. 11, no. 11, pp. 887–890, 2004.

[31] Y. Z. Jiao, X. J. Liu, and X. A. Wang, "A novel tone reservation scheme with fast convergence for papr reduction in ofdm systems," in *2008 5th IEEE Consumer Communications and Networking Conference*, 2008, pp. 398–402.

[32] T. Jiang, C. Ni, C. Xu, and Q. Qi, "Curve fitting based tone reservation method with low complexity for papr reduction in ofdm systems," *IEEE Communications Letters*, vol. 18, no. 5, pp. 805–808, 2014.

[33] E. Tampubolon and H. Boche, "Probabilistic analysis of tone reservation method for the papr reduction of ofdm systems," in *2017 IEEE International Conference on Acoustics, Speech and Signal Processing (ICASSP)*, 2017, pp. 3799–3803.

[34] W. Henkel, A. Wakeel, and M. Taseska, "Peak-to-average ratio reduction with tone reservation in multi-user and mimo ofdm," in *2012 1st IEEE International Conference on Communications in China (ICCC)*, 2012, pp. 372–376.

[35] M. Eyuboglu and G. Forney, "Trellis precoding: combined coding, precoding and shaping for intersymbol interference channels," *IEEE Transactions on Information Theory*, vol. 38, no. 2, pp. 301–314, 1992.

[36] G. Forney, "Trellis shaping," *IEEE Transactions on Information Theory*, vol. 38, no. 2, pp. 281–300, 1992.

[37] H. Ochiai, "A novel trellis-shaping design with both peak and average power reduction for ofdm systems," *IEEE Transactions on Communications*, vol. 52, no. 11, pp. 1916–1926, 2004.

[38] R. Yoshizawa and H. Ochiai, "Performance comparison of trellis-shaped ofdm systems over nonlinear channels," in *2011 The 14th International Symposium on Wireless Personal Multimedia Communications (WPMC)*, 2011, pp. 1–5.

[39] M. Tanahashi and H. Ochiai, "Near constant envelope trellis shaping for psk signaling," *IEEE Transactions on Communications*, vol. 57, no. 2, pp. 450–458, 2009.

[40] D. Jones, "Peak power reduction in ofdm and dmt via active channel modification," in *Conference Record of the Thirty-Third Asilomar Conference on Signals, Systems, and Computers (Cat. No.CH37020)*, vol. 2, 1999, pp. 1076–1079 vol.2.

[41] B. Krongold and D. Jones, "Par reduction in ofdm via active constellation extension," *IEEE Transactions on Broadcasting*, vol. 49, no. 3, pp. 258–268, 2003.

[42] G. Woo and D. Jones, "Peak power reduction in mimo ofdm via active channel extension," in *IEEE International Conference on Communications, 2005. ICC 2005. 2005*, vol. 4, 2005, pp. 2636–2639 Vol. 4.

[43] W. Henkel and B. Wagner, "Another application for trellis shaping: Par reduction for dmt (ofdm)," *IEEE Transactions on Communications*, vol. 48, no. 9, pp. 1471–1476, 2000.

[44] T. T. Nguyen and L. Lampe, "Trellis shaping for par reduction in ofdm systems," in *2006 IEEE International Conference on Communications*, vol. 10, 2006, pp. 4670–4675.

[45] G. Forney, R. Gallager, G. Lang, F. Longstaff, and S. Qureshi, "Efficient modulation for band-limited channels," *IEEE Journal on Selected Areas in Communications*, vol. 2, no. 5, pp. 632–647, 1984.

[46] K. Paterson, "Generalized reed-muller codes and power control in ofdm modulation," *IEEE Transactions on Information Theory*, vol. 46, no. 1, pp. 104–120, 2000.

[47] H. Imai and S. Hirakawa, "A new multilevel coding method using error-correcting codes," *IEEE Transactions on Information Theory*, vol. 23, no. 3, pp. 371–377, 1977.

[48] W. Yu, D. Varodayan, and J. Cioffi, "Trellis and convolutional precoding for transmitter-based interference presubtraction," *IEEE Transactions on Communications*, vol. 53, no. 7, pp. 1220–1230, 2005.

[49] G. Forney and L.-F. Wei, "Multidimensional constellations. i. introduction, figures of merit, and generalized cross constellations," *IEEE Journal on Selected Areas in Communications*, vol. 7, no. 6, pp. 877–892, 1989.

[50] H. Ochiai and H. Imai, "On the distribution of the peak-to-average power ratio in ofdm signals," *IEEE Transactions on Communications*, vol. 49, no. 2, pp. 282–289, 2001.

[51] R. Tanner, "A recursive approach to low complexity codes," *IEEE Transactions on Information Theory*, vol. 27, no. 5, pp. 533–547, 1981.

[52] L. Bahl, J. Cocke, F. Jelinek, and J. Raviv, "Optimal decoding of linear codes for minimizing symbol error rate (corresp.)," *IEEE Transactions on Information Theory*, vol. 20, no. 2, pp. 284–287, 1974.

[53] T. Richardson, M. Shokrollahi, and R. Urbanke, "Design of capacity-approaching irregular low-density parity-check codes," *IEEE Transactions on Information Theory*, vol. 47, no. 2, pp. 619–637, 2001.

[54] N. von Deetzen and S. Sandberg, "On the uep capabilities of several ldpc construction algorithms," *IEEE Transactions on Communications*, vol. 58, no. 11, pp. 3041–3046, 2010.

[55] S. Sandberg and N. Von Deetzen, “Design of bandwidth-efficient unequal error protection ldpc codes,” *IEEE Transactions on Communications*, vol. 58, no. 3, pp. 802–811, 2010.

[56] T. Richardson and R. Urbanke, “The capacity of low-density parity-check codes under message-passing decoding,” *IEEE Transactions on Information Theory*, vol. 47, no. 2, pp. 599–618, 2001.

[57] A. Wakeel, W. Henkel, and F. Gao, “Effect of the threshold offset on the performance of uep ldpc codes,” in *2013 IEEE/CIC International Conference on Communications in China (ICCC)*, 2013, pp. 50–54.

[58] A. Filip and W. Henkel, “Hierarchical modulation to support low-density parity-check code design?” in *SCC 2013; 9th International ITG Conference on Systems, Communication and Coding*, 2013, pp. 1–6.

[59] D. Yoon, K. Cho, and J. Lee, “Bit error probability of m-ary quadrature amplitude modulation,” in *Vehicular Technology Conference Fall 2000. IEEE VTS Fall VTC2000. 52nd Vehicular Technology Conference (Cat. No.00CH37152)*, vol. 5, 2000, pp. 2422–2427 vol.5.

[60] S.-Y. Chung, T. Richardson, and R. Urbanke, “Analysis of sum-product decoding of low-density parity-check codes using a gaussian approximation,” *IEEE Transactions on Information Theory*, vol. 47, no. 2, pp. 657–670, 2001.

[61] R. Yoshizawa and H. Ochiai, “A trellis shaping for peak and average power reduction of bicm-ofdm signals,” *IEEE Transactions on Wireless Communications*, vol. 14, no. 2, pp. 1143–1154, 2015.